UNIVERSIDAD DE INVESTIGACIÓN DE TECNOLOGÍA EXPERIMENTAL YACHAY

Escuela de Ciencias de la Tierra, Energía y Ambiente

TÍTULO: Mineralogical characterization of alluvial gold mining tailings in the north of the country.

Trabajo de integración curricular presentado como requisito para la obtención del título de Geólogo

Autor:

Fajardo Tenesaca Paul

Tutora:

MSc - Rodríguez Calvopiña Mariela

Co-tutor:

PhD - Vázquez Taset Yaniel

Urcuquí, Diciembre 2023

Autoría

Yo, **PAUL FERNANDO FAJARDO TENESACA**, con cédula de identidad 0106772908, declaro que las ideas, juicios, valoraciones, interpretaciones, consultas bibliográficas, definiciones y conceptualizaciones expuestas en el presente trabajo; así cómo, los procedimientos y herramientas utilizadas en la investigación, son de absoluta responsabilidad de el autor del trabajo de integración curricular. Así mismo, me acojo a los reglamentos internos de la Universidad de Investigación de Tecnología Experimental Yachay.

Urcuquí, Septiembre 2023.

_____

Fajardo Tenesaca Paul Fernando

CI: 0106772908

Autorización de publicación

Yo, **Fajardo Tenesaca Paul Fernando**, con cédula de identidad 0106772908, cedo a la Universidad de Investigación de Tecnología Experimental Yachay, los derechos de publicación de la presente obra, sin que deba haber un reconocimiento económico por este concepto. Declaro además que el texto del presente trabajo de titulación no podrá ser cedido a ninguna empresa editorial para su publicación u otros fines, sin contar previamente con la autorización escrita de la Universidad.

Asimismo, autorizo a la Universidad que realice la digitalización y publicación de este trabajo de integración curricular en el repositorio virtual, de conformidad a lo dispuesto en el Art. 144 de la Ley Orgánica de Educación

Urcuquí, Septiembre 2023.

<div align="center">

_____

Paul Fernando Fajardo Tenesaca

CI: 0106772908

</div>

Dedication

A mis queridos padres Alfonso y Elvia,

Soy la historia que comenzaron, soy el esfuerzo y la dedicación que me enseñaron, soy el amor incondicional que me dan todos los dias, soy lo que soy gracias a ustedes y a todo lo que dejan en mi.

Esta tesis lleva su nombre como un recordatorio de que soy lo que soy gracias a su inmenso amor.

A mi querida familia,

Sus risas, su apoyo y su comprensión han sido mi refugio en momentos de dificultad. A mis tías Luzma, Rebeca y Elsa, gracias por ser mi eterno soporte. Tambien a mi querido tío Ariosto y Janeth, gracias por estar para mi en estos años y darme mi segundo hogar.

A mi querida Vicky,

Tu amor y paciencia han sido luz en los días más oscuros de mi viaje académico. Tu apoyo inquebrantable y tu presencia constante me han sostenido en cada paso del camino. Gracias por tanto mi Tataya.

A mis amigos,

La vida universitaria no habría sido la misma sin ustedes. Sus risas, consejos y momentos compartidos han hecho que este viaje sea inolvidable. Esta tesis es un tributo a nuestra amistad duradera.

A mis respetados profesores,

Su sabiduría, paciencia y guía experta me han moldeado como estudiante y como persona. Estoy profundamente agradecido por las lecciones que he aprendido bajo su tutela.

Esta tesis es el resultado de los esfuerzos combinados de todos ustedes. A cada uno de ustedes, les dedico este logro con gratitud y cariño.

Con amor y gratitud, Paul Fernando.

Acknowledgment

Resumen

En Ecuador existen cinco distritos mineros: Esmeraldas, Daule - Quevedo, Puyango - Balao, Zamora Chinchipe - Upano y Paztaza. Uno de los puntos mineros más antiguos del norte de Ecuador son los yacimientos aluviales del Río Santiago, ubicados en la provincia de Esmeraldas. La Región Costera está formada por muchas cuencas donde se depositaron materiales ricos en forma de estribaciones y abanicos aluviales; estos sedimentos contienen minerales preciosos. Sin embargo, las operaciones mineras artesanales se habían centrado únicamente en la extracción de oro aluvial. El objetivo de esta investigación es identificar los minerales económicamente valiosos presentes en las arenas. Estas arenas son el subproducto o residuo de las actividades mineras artesanales de la región. Además, este trabajo pretende aportar información valiosa sobre el desarrollo de la minería artesanal e ilegal en el país, así como sobre los minerales que se extraen y los que aún quedan por explotar en esta actividad. Para alcanzar estos objetivos, se llevaron a cabo análisis detallados de muestras mediante diversas técnicas analíticas, como el recuento puntual y la mineralogía descriptiva. También se emplearon técnicas ópticas avanzadas, como la difracción de rayos X (DRX), la espectroscopia Raman para sedimentos, la espectroscopia de fotoelectrones de rayos X (XPS), la espectrometría de masas con plasma acoplado inductivamente (ICP-MS) y la espectroscopia de emisión óptica con plasma acoplado inductivamente (ICP-OES). Los resultados revelaron hallazgos significativos, entre ellos se identificó la presencia de minerales de platino, minerales ricos en aluminio y magnesio, y minerales ricos en hierro en las muestras analizadas en la zona del Río Santiago, en la provincia de Esmeraldas. Otro aporte interesante es la presencia de todos los Elementos Raros de la Tierra (REE), predominando los valores de Lantano, Cerio y Neodimio. Estos hallazgos muestran que minerales económicamente valiosos podrían ser objeto de futuras investigaciones y exploraciones. En resumen, este trabajo de investigación pone de relieve la necesidad de abordar cuestiones relacionadas con la sostenibilidad y la regulación en este sector. Además, los resultados sugieren la posibilidad de descubrir nuevas

fuentes de minerales valiosos en la zona, lo que abre oportunidades para futuras investigaciones en busca de metales preciosos y recursos minerales estratégicos.

Palabras Clave:

Minería artesanal, arenas aluviales, caracterización mineralógica, elementos de tierras raras, minería metálica, desarrollo sostenible.

Abstract

In Ecuador, there are five mining districts: Esmeraldas, Daule - Quevedo, Puyango – Balao, Zamora Chinchipe – Upano, and Paztaza. One of the oldest mining spots in northern Ecuador is the Santiago River alluvial deposits, located in Esmeraldas province. The Coastal Region is formed by many basins where rich materials were deposited as foothills and alluvial fans; these sediments contain precious minerals. However, artisanal mining operations had focused on the extraction of alluvial gold only. This research aims to identify economically valuable minerals present in the sands. These sands are the byproduct or waste of artisanal mining activities in the region. Additionally, the project seeks to provide valuable insights into the development of artisanal and illegal mining in the country, as well as the minerals being extracted and those yet untapped in this activity. To achieve these objectives, detailed analyses of samples were conducted using various analytical techniques, including point counting and descriptive mineralogy. Advanced optical techniques were also employed, such as X-ray Diffraction (XRD), Raman Spectroscopy for sediments, X-ray Photoelectron Spectroscopy (XPS), Inductively Coupled Plasma Mass Spectrometry (ICP-MS), and Inductively Coupled Plasma Optical Emission Spectroscopy (ICP-OES). The results revealed significant findings, including the presence of Platinum minerals, minerals rich in aluminum and magnesium, and iron-rich minerals in the analyzed samples in the Santiago River area of Esmeraldas. Another interesting contribution is the presence of all the Rare Earth Elements (REE), predominating values of lanthanum, cerium, and neodymium. These findings indicate that economically valuable minerals could be subject to future investigations and exploration. In summary, this research project highlights the need to address issues related to sustainability and regulation in this sector. Furthermore, the results suggest the potential for discovering new sources of valuable minerals in the area, opening up opportunities for future research in the quest for precious metals and strategic mineral resources.

Keywords:

Artisanal Mining, Alluvial Sands, Mineralogical Characterization, Rare Earth Elements, Metallic Mining, Sustainable Development.

Contents

List of Tables

List of Figures

Chapter 1

Introduction

1.1 Background

Ecuador is located on the western side of the South American continent, forming a part of the well-known Pacific Ring of Fire and the northern Andes Mountain Range. The northern Andes occupy the territory from Cajamarca (northern Peru), crossing Ecuador and Colombia until Panama. The interaction of the South American plate, which overthrust the Nazca, Cocos, and Caribean Plates, characterizes the tectonic setting of the region. Because of such interaction, a subduction zone is created, resulting in the Andean Orogeny, which also separates the coastal region to the west from the Amazon region on the east [Pillajo Gavidia, 2008].

The Andes is a colossal mountain barrier approximately 100 to 120 km wide extending from Panama in the north to the south of Argentina, running approximately 7000 km along Western South America (Fig. 1.1). Its higger peak is the Aconcagua (6961 masl), located in Argentina. According to Pillajo Gavidia (2008), the Andes present recent and more robust volcanic activity in the north, forming prominent volcanic edifices (>4500m height), which constitute the Oriental and Real Cordillera (Fig. 1.2a). To the south, the volcanic activity is almost gone, and volcanoes (>4000m) disappear because of the high exposure to the elements. The erosive processes in the southern mountains provide detrital materials to the western and eastern flanks of the Cordillera. The depositional environment for the transported sediments is located in the coastal and Amazon zones with distinguishable low relief and deep valleys [Barragan et al., 1991, Tamay, 2018].

1

Figure 1.1: Map of The Andes Orogeny along western South America from Panama to Argentina.

The coastal (western) part of the Andean Cordillera is formed by many basins where rich materials were deposited as foothills and alluvial fans [Pillajo Gavidia, 2008]. The sediments from the highlands contain precious minerals that people may extract. The extraction of gold from alluvial deposits in Ecuador is mainly artisanal and is developed by people living near the rivers. Those auriferous rivers are precious, and, according to the regulation agency, in our country, we have five delimited mining districts: Esmeraldas – Santiago, Daule – Quevedo, Puyango - Balao, Zamora Chinchipe – Upano, and Pastaza – Aguarico [Ministerio del Ambiente, 2020].

One of the oldest mining spots in northern Ecuador is the Santiago River alluvial deposits, located in Esmeraldas province. These deposits are distributed along the border of San Lorenzo and Eloy Alfaro cantons, inside the Esmeraldas – Santiago district (Fig. 1.2b). According to Pillajo Gavidia (2008), the relative amount of minerals along the district is variable; however, the important part is that they have found gold in every

sample. The gold and other materials found in the deposits are believed that come from the green and volcano-sedimentary rocks of Macuchi and Cayo de la Sierra units, from acidic to ultrabasic intrusions, and from magmatic deposits such as veins; all of them located in the Cordillera [Pillajo Gavidia, 2008].
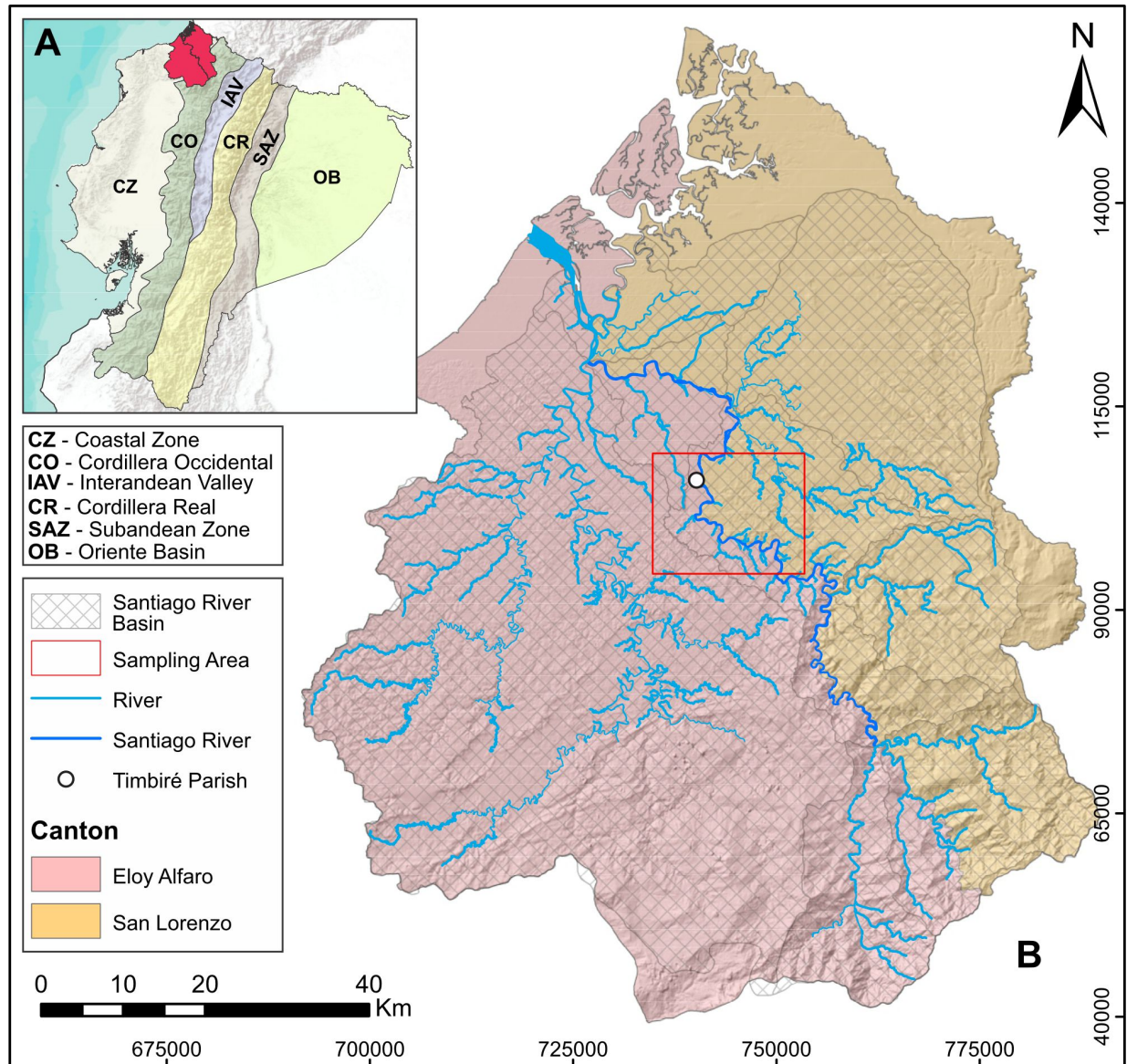
Figure 1.2: Location of the study area inside the Santiago River watershed, in Esmeraldas Province.

According to Lucero (2018), the study zone outcrops some tertiary and quaternary sedimentary rock units from the high Eocene to Pleistocene in age; there is evidence that these rocks are laying over Cretaceous marine basalts. The basement of the zone is recognized as the Piñon formation, over which a high thickness of marine rocks, carbonates,

and reef residuals from Tertiary shallow water [Lucero, 2014].

The sediments deposited over time and at different epochs in a marine environment had folded, fractured, and faulted due to compressive events and orogeny. That is why we should find sedimentary outcrops with different rock types. Finally, at the top, we have a sedimentation pack composed of volcanic clasts, granodiorites, porphyries, breccias, and a clay-sand matrix that contains minerals of interest such as gold, platinum, magnetite, ilmenite, and others [Lucero, 2014].

1.2   The problem of artisanal mining in the north of Ecuador

According to the ARCOM (Agencia de Regulación y Control Minero), the regulatory agency for small and big-scale mining, artisanal gold exploitation in Ecuador has been one of the primary sources of employment and money for many people. The lack of technology and knowledge, the usage of old processes, the lousy job environment, and illegality are the problems that artisanal mining faces [Ministerio del Ambiente, 2020]. The problem becomes more significant when considering the contamination that artisanal mining lefts behind. According to MAE (2020), artisanal mining extracts a big part of the gold in Ecuador, having 1821 licenses for metallic mining (Fig. 1.3); however, controlling the activity on its total is difficult.

These deposits have been exploited since the colony by enslaved people from abroad and indigenous people from the zone; they explored the river basin to extract gold. Nowadays, small and big plants use the same old mining techniques to extract the mineral with mercury (Hg) and cyanide [Barragan et al., 1991]. Apart from the environmental effect, it is known that these methods need to be improved for extracting all the minerals and metals. Therefore, artisanal mining is wasting what can be a potential source for extracting minerals other than gold.

Figure 1.3: Photography published by Primicias EC (primicias.ec), an online journal of Ecuador. It shows how in San Lorenzo Canton, the illegal mining activity has grown, having big machinery and people working to extract the metal-rich material from the alluvial deposits on riverbanks.

The regularization and management of small-scale mining are complicated because many people are doing the activity, and the information is scarce. For example, according to Pillajo Gavidia (2008), Santiago river is only reported to have gold and platinum exploitation. However, some other minerals in the sands of the Santiago River were found [López-Males et al., 2020]. Hence, the possibility of having good mineral deposits (other than gold) is high, and their identification will help to improve the regularization, reducing the illegality and environmental damage.

1.3   Purpose

The purpose of this work is to give detailed information on the mineralogical composition of the material present in one of the areas with greater artisanal exploitation of the country, to determine if the minerals found are of economic interest, and finally, to determine the presence of rare elements in the mining sectors located along the rivers in northern Ecuador.

1.4   Motivation

The motivation to carry out this research comes from the care for Ecuador's resources. In this way, we try to show the true potential of our mining sectors, promoting clean mining and focusing on the same environmental and economic objectives.

1.5   Objectives

1.5.1   General Objective

- To characterize the minerals of alluvial gold mining tailings in the northern zone of Ecuador.

1.5.2   Specific Objectives

- Through analytic methods, determine the presence of minerals of economic and industrial interest in the tailings left by artisanal mining.

- Perform a mineralogical characterization and analysis to find and identify which fraction accumulates the most considerable amount of interest minerals.

- Determine whether the samples have REE and where minerals are found, if present.

1.6   Limitations and resources

The primary constraint of this study was the collection of samples and the local geology. Due to the study site being situated within an artisanal mining zone, significant security concerns hindered the ability to access the area, gather samples, and accurately describe the geological features present. For this reason, the samples were extracted by collaborators; consequently, a detailed stratigraphic description and mapping of the terraces were impossible to carry out.

Hence, the study was constrained by the university's available analytical resources and the collaborative efforts of the University of Granada, which was responsible for conducting the ICP analyses.

Chapter 2

Literature Review

2.1 The general geologic and mineralogical context of the zone

With the objective of having a background in what minerals should be expected in the samples, a general description of the materials along the Santiago River is made.

2.1.1 Alluvial terraces

Alluvial materials such as gravel and sand have been deposited on the banks of Santiago River, and all the drainages that make up the coastal hydrographic network of the province of Esmeraldas, forming islets, river beaches, or terraces, the latter reaching heights of 7m above the river level [Lucero, 2014].

According to the literature, alluvial flood fan deposits are arranged along the Santiago River basin, mostly forming vast flood plains with gravel deposits within a sandy matrix and lenticular sand intercalations. Lucero (2014) found that the boulders are rounded to sub-rounded, from centimeters to occasional meters in size (Fig. 2.1). Lithologically, clasts of volcanic origin predominate, such as andesites, tuffs, porphyrites, basalts, scarce granodioritic intrusives, and, in a lesser proportion, red and black jaspers and scarce quartz. Finally, as last-generation deposits, vast areas are covered by sandy-loamy bluish-gray color in lenses of 1 to 2 m and intercalations of gray clays. These events are frequent in the lower strata, where, due to a decrease in slope and the presence of flat features, flooding and discharge of the fluvial-transported sediments occur [Lucero, 2014].
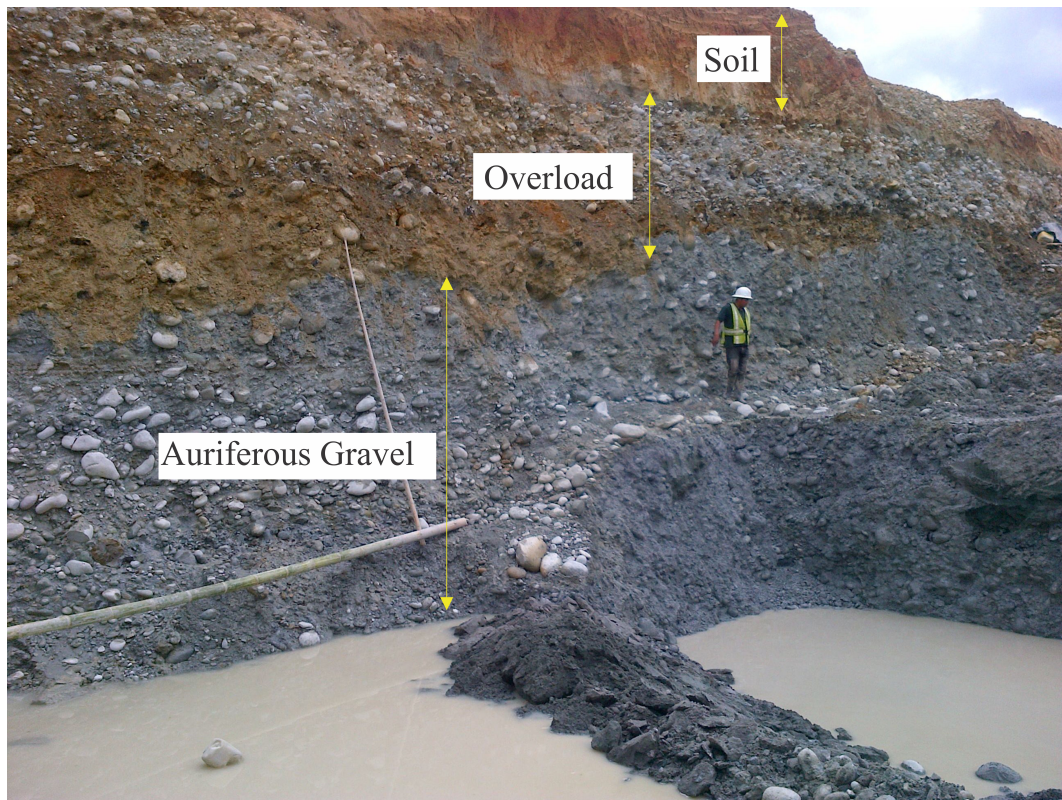
Figure 2.1: Image of the sample source. Components of the alluvial deposits are shown in cross-section photography. Using the person as scale, it can be observed that the auriferous gravel layer (mineral-rich gravel) is potent and covered by a thick overload and soil components.

2.1.2 Riverbank deposits

During the advanced exploration stage carried out by Lucero (2014), some relevant information has served to estimate the characteristics of the deposit. They have found that the types of boulders generally correspond to gray andesitic rocks, volcanic breccias, mineralized hydrothermal breccias, greenish volcanic rocks mineralized with sulfides (oxidized on the surface), kaolinized porphyries, porphyries mineralized with sulfides, small red and black jaspers; in minor occurrence are observed rolled intrusive rocks, with crystals developed in some cases of hornblende, quartz, feldspars (granodiorites); also are observed scarcely rolled carbonate rocks with macroscopic fossils.

In the same way, they found that gold and platinum are present in the sandy-clay matrix, a component of the gravel stratum. The precious metal is dispersed, mostly in laminar form but also in granular form, with dimensions greater than 2 millimeters and visible with a magnifying glass [Lucero, 2014]. At the same time, platinum is found in

a meager percentage in relation to gold, and its sparks are visible with a magnifying glass [Weiser and Schmidt-Thome, 1993]. Due to its geometric characteristics, the Santiago deposit has been defined as a horizontal deposit of flat surface, composed of a vegetal layer whose covering power goes from 0.20 to 0.50 m and clay with a thickness that varies from 0.80 to 2.00 m. As usable material, there is an estimated thickness of auriferous gravels from 2 to 10 meters deep [Lucero, 2014], as shown in Fig. 2.1.

The bedrock corresponds to consolidated sandstones in a blue-grayish silty clay matrix with marine fossils, estimated to correspond to the Borbón Formation. This stratum has a negligible or almost null presence of gold; nevertheless, in the mining phase, it is extracted approximately 8 cm of the same one since, in the presence of fissures or discontinuities, an accumulation of gold can exist [Lucero, 2014].

In this way, the mineral-rich alluvial deposits are distributed over a long area following the river course; in Figure 2.2, we can observe the distribution of the geological features that underlies the valuable material. We can observe 5 formations that outcrop in the area. According to the Stratigraphic Lexicon of Ecuador compiled by Duque (2000) and the detailed description of the intramountainous basins of The Andes published by Tamay (2018), from older to younger, we have:

- **Zapallo Formation:** Corresponding to the Eocene, a striking SW-NE body is composed of pale grey hard shales with foraminifera. At the bottom, there are a lot of tuffs and siliceous clays. It lays discordantly over Piñon Fm and Santiago Fm. It is covered discordantly by Playa Rica formation.

- **Playa Rica Formation:** Corresponding to the Oligocene, this formation strikes SW-NE. At the base, a thick conglomerate with Cretaceous volcanic clasts and Santiago Fm limestones. Generally, it comprises grey to black shales, hard, laminated, foraminifera, with sandstone intercalations. It is discordant with the underlying Santiago Fm and Zapallo Fm. It contains a lot of fossils, such as Brachiopods, Echinoderms, mollusks, and planktonic fossils.

- **Angostura Formation:** Corresponding to the Upper Miocene, its outcropping rocks are striking to the SW and dipping to the center of the basin. It represents a

transgressive and sublittoral origin. Formed by a basal conglomerate with volcanic clasts and continues with sandstones of variable grain size and marine mollusk fossils.

- **Onzole Formation:** Corresponding to the Lower Miocene composed mainly of blue siltstones, silty shales, and a few conglomerates and sandstones. In some areas, they are a lot of mollusk fossils. It is lying over Angostura Fm with a concordant contact.

- **Borbon Formation:** Corresponding to the Lower Pliocene is the younger formation composed of a basal conglomerate that overlies over the Onzole and Playa Grande Fm with a discordant contact. Then a coarse-grained sandstone with mollusk megafossils corresponding to marine facies.
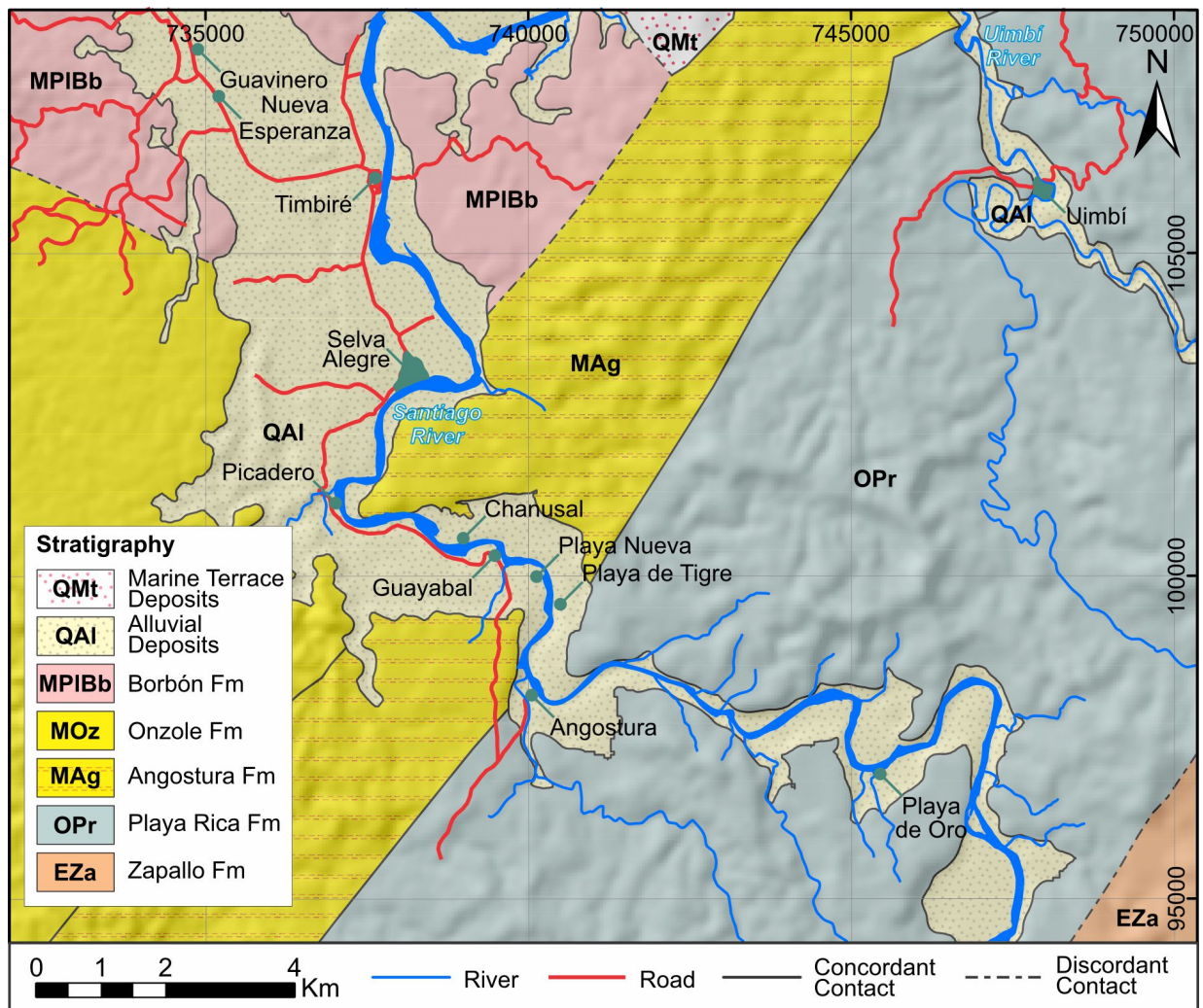
Figure 2.2: Geologic features of the area of study where the mineral-rich alluvial terraces are lying. See location on Figure 1.2.*Map modified from ENAMI EP (2016) by Fajardo P.*

2.2   Mineralogical characterization of alluvial sands

The bibliography refers to the Santiago River surrounding areas as a mineral-rich material with high economic interest; for this reason, some studies had been made in the terraces previously.

2.2.1   Previous mineralogical studies

Previous studies have been made studying the mineralogy of Santiago River sediments. Lucero G. (2014) carried out a descriptive analysis of the minerals encountered in samples from a riverbank. They did an XRD analysis for samples coming from the head, tailing, and concentrated materials of the gold extraction process. The results of the analysis gave them a clear idea of the mineral composition of the samples, having: quartz (17%), plagioclase group (40%), Muscovite (9%), Vermiculite (1%), Cordierite (2%), Kaolinite (18%), among others (Lucero, 2014). Then, by melting the samples to separate metals, they calculated the number of minerals of economic interest, such as gold (0,018 g/m3), silver (21.6 g/m3), and platinum (0.018 g/m3).

The deposits of the Santiago River, in which the artisanal activity develops, are mainly flooding terraces, lateral accretion (bars), and hanging terraces [Pillajo Gavidia, 2008]. The extraction of metals from these deposits leaves a massive amount of material on the riversides. Modern tools can recognize which minerals may be in these residual materials. Therefore, this work intends to sample the material left on the riverside and then, using physical and optical methods (available at Yachay Tech), separate, analyze and determine the mineralogical composition that Santiago River tailings have. Consequently, having a statistical analysis of the results, we can state whether Santiago River is or not a potential source of minerals of industrial or economic interest.

Chapter 3

Methodology

During the several months it took to develop this work, many analyses and comparisons were made to have the best data quality. The analyses, except the ICP-MS/OES, were made in Yachay Tech laboratories and using the available instruments. Gratefully, all of them gave us some nice and essential results. This section describes the workflow that was carried out for the samples:

3.1 Sampling

Santiago River is depositing sediments on the riverbanks along a big area where mining is being developed as an illegal activity (Fig. 1.3. For this work's reference, exploitation occurs near the Timbiré parish on the border between San Lorenzo and Eloy Alfaro cantons (Fig. 1.2b). Around this place, most mining projects cut tens of meters of riverbank deposits to extract the buried sediments (Figs. 2.1 and 1.3). The raw gravels are then processed in a "Z" shaped ore chute where the coarser material is trapped in the hopper and separated from the finer material, which descends by a channel that separates the heavy material, which contains gold, from the lighter one. Once the chute extracts the gold, the tailing sediment is collected, and an operator extracts the remaining gold by panning.

The samples analyzed in this work come from a riverbank in which a 900 m^2 area and 10 m depth pool were cut. Therefore, 9000 m^3 of sediments were processed following the previously described separation method. From the tailings of the ore chute, two groups of samples were acquired and classified:

1. Dark Samples

   - This will describe the samples that are the final concentrated material of the tailing after the extraction of gold by panning. There are dark in color because of the high content of heavy black materials that accompany gold particles.

2. Light Samples

   - The samples described as light samples are the residue without the panning, the lighter material that came out directly from the ore chute.

The sample coding in Table 3.1 separates each sample by its type:

Table 3.1: Classification of the samples by their type, dark samples are concentrated in heavy minerals through a panning process, while light samples are the material that comes from the ore chute where the heavy minerals are separated.

Light	Dark
PE-003	PE-001
PE-005	PE-002
PE-007	PE-004
PE-009	PE-006
	PE-008
	PE-010

3.2   Physical analysis

In this section, the samples went through methods to separate them into fractions with the same physical characteristics. These techniques take advantage of the gravity force and magnetic properties of the sand to separate the samples into smaller fractions, which optical instruments will analyze later.

3.2.1   Drying

Separating the gold-bearing sediment through channels uses the drag of water to move the light particles and leave the concentration of heavy material. The samples used are tailings from this process and contain much moisture; for this reason, it is essential to dry the samples. For this work, the samples went through a 4-day drying process.

Each wet sand sample was placed inside individual borosilicate glass crystallizers to have control of the vessel weight (Fig. 3.1a). The containers were labeled using tape and coding. Then, the containers were placed in a Selecta Professional oven set at 100 °C (Fig. 3.1b). The samples were subjected to heat periods of 8 hours per day for four days.
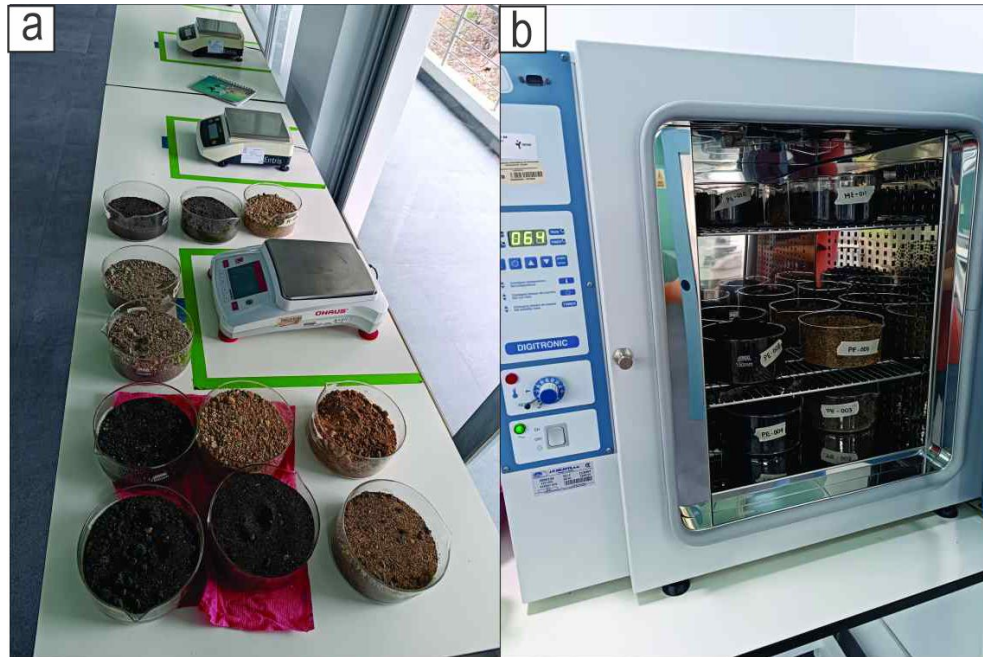
Figure 3.1: a) Sample weighting and labeling. b) Selecta Professional oven set to 100 °C.

After drying, the weights presented in Table 3.2 were obtained, and each sample's percentage of water contained was also reported. In order to make the analysis as homogeneous as possible, 800 g of each dry sample was taken, labeled, and passed to the following stage of granulometric characterization.

3.2.2 Granulometric separation (Sieving)

The sediments in which interest minerals are contained are constituted of different-sized grains. The grain size of the particles determines the quality of the results from the operations with the samples in the following steps. It is common to determine the grain size of a bulk sample by using the d_{80} value, which is the size of the sieve that lets the 80% of the material pass [Londoño et al., 2010]. In this way, we used a professional sieving machine that separates grains in a dry environment (Fig. 3.2) through the vibration that carries the material through the nets.

Table 3.2: Measured weights of each sample after the drying process. The table also shows the sample's original water content calculation.

Initial Weight (g)	4-day dry weight (g)	Water Content
1734.56	1548.97	11%
1864.66	1653.11	11%
1541.53	1345.76	13%
1960.04	1758.25	10%
1195.77	962.3	20%
1618.77	1461.42	10%
1329.07	1147.27	14%
2448.37	2307.4	6%
1122.58	957.77	15%
1934.14	1755.08	9%

For the granulometric analysis by sieving, the material is passed through a series of sieves with nets of different sizes; as a result, the fraction of particles with grains bigger than the net size will be retained (Fig. 3.3). According to Londoño et al. (2010), there are ways to force the material through the nets by using water to drag and separate small particles attached to the bigger ones. On the other hand, the dry method compensates for the water dragging by having a longer shaking time, but still, some error is expected.

Procedure

The ten samples were separated on a sieving machine with six different-sized sieves from 10 MESH or 2 mm to 230 MESH or 63 µm (Fig. 3.2). Each sample was processed for 40 minutes, then the fractions were labeled and stored, and finally, the entire set of sieves must be immaculately clean to receive the next one (Fig. 3.3). Using an ultrasonic cleaner, all the particles trapped somewhere in the sieves were retired to get the set ready again. Once the ten samples were separated, the fractions were weighted, and the value of d_{80} was computed.

3.2.3   Magnetic separation

The magnetic separation of sands aims to identify and separate fractions of material to identify each mineral's proportions within the samples. In this case, an attempt is made to separate each sample's magnetic, paramagnetic, and diamagnetic parts. According to Londoño et al. (2010), this type of separation, in the industrial field, is highly used to

	mm	µm
10 MESH	2	2000
18 MESH	1	1000
35 MESH	0.5	500
60 MESH	0.25	250
120 MESH	0.125	125
230 MESH	0.063	63

Figure 3.2: Sieving machine for the granulometric separation of the sands. Each level has its net size from 10 MESH to 230 MESH (the values in μm are reported in the attached table. The sand particles are separated by size using the vibration of the machine's base and passing through a series of fine nets.

produce raw materials based on iron-containing materials. In our case, it is performed within the laboratory to characterize minerals that occur as companions of gold. This technique is primarily applied to identify gold-bearing minerals and the so-called black sands, mainly composed of polymetallic sulfides.

The analysis is based on each mineral's magnetic susceptibility, defined as the material's response when a particular magnetic field is applied to it [Rosenblum and Brownfield, 1999]. This way, we can induce a controlled magnetic field to each sand sample, which will be fractionated according to its properties, resulting in a controlled and accurate separation of mineral phases. This process is time-consuming and tedious since it involves passing single mineral particles through an inclined and magnetized vibrating channel, which confines the grains to move with a constant velocity. The configuration of the inclination angles, the magnetic field's intensity, and the movement speed group the minerals with the same magnetic susceptibility and separate them from the others.
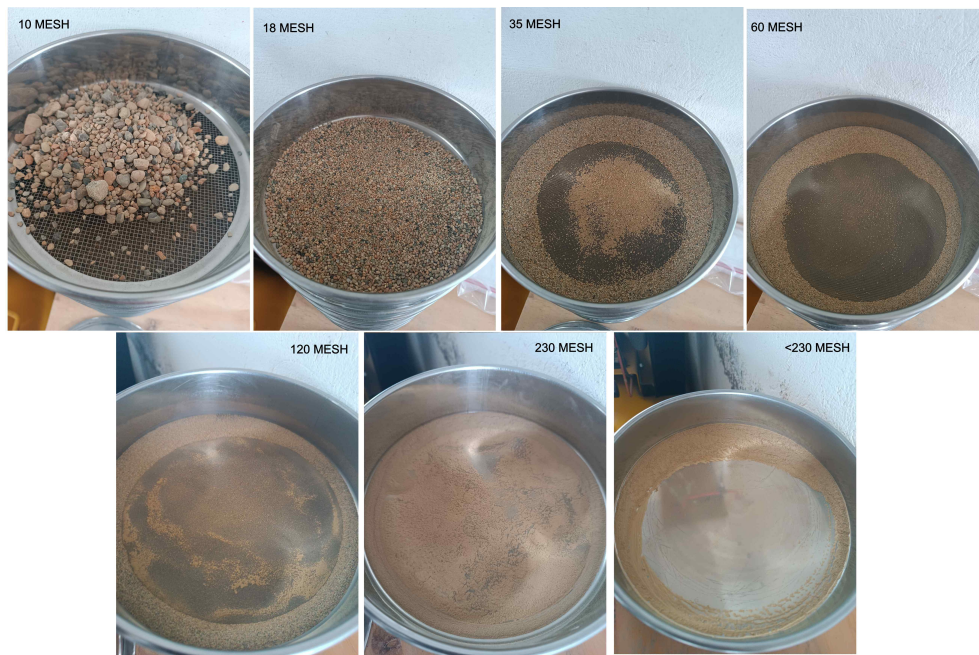
Figure 3.3: Example of the sieving process carried out in the sample PE-003 where the size of its particles separated seven different fractions. Each container has its net with a certain size from 10 MESH to 230 MESH.

Londoño et al. (2010) and Rosenblum & Brownfield (1999) present susceptibility data for many minerals, separating them into ferromagnetic, paramagnetic, and diamagnetic. Ferromagnetic minerals constitute the group of minerals that are attracted by a magnet, which produces a magnetic field between 0.1 and 0.3 amperes (amp) [Londoño et al., 2010], being the most common minerals: Magnetite, Maghemite, Pyrrhotite, and Pentlandite [Rosenblum and Brownfield, 1999]. Paramagnetic minerals refer to minerals whose response is lower than ferromagnetic minerals [Rosenblum and Brownfield, 1999] and have a response to magnetic fields between 0.4 and 1.7 amps, the most common mineral being Ilmenite [Londoño et al., 2010]. Finally, diamagnetic minerals do not show magnetism at 1.7 amps and usually show repulsion to electromagnets with higher intensities.

Equipment

A Frantz LB-1 isodynamic equipment was used in the laboratory to fractionate the samples by magnetic separation, feeding through a separating channel inclined at 30º laterally and 15º frontally (Fig. 3.4).

Figure 3.4: Magnetic separator Frantz model LB-1. It consists of a strong electromagnet that can produce controlled magnetic fields around a channel between two large magnets and a current and voltage regulator that allows us to control and monitor the magnetic field in which we separate our samples.

Procedure

The equipment works by fulfilling three conditions that were adapted during the process to get the best performance on our separation:

- The grain size that the separating channel admitted.

- The amount of material the feeding cone sends to the channel.

- The intensity of the vibrations.

These conditions must be respected since one variation changes the flow velocity, causes obstructions, and contaminates the separated fractions. For this reason, the separation process took a long time to achieve an optimal calibration between the material amount and vibration intensity to have the maximum and best fractionation of the samples. Once these parameters were determined, all the samples were processed at different magnetic field intensities.

1. Since the separator presented obstructions with the raw material, we started separating the ferromagnetic materials with the help of a neodymium magnet; in this phase, we separated mostly Magnetite.

2. Once the ferromagnetic materials were separated, the Frantz was initialized at an initial current intensity of 0.3 amps, which increased to 0.8 amps in 3 repetitions to separate the paramagnetic minerals according to the protocol presented by Londoño et al. (2010).

3. A new run is performed with an intensity of 1.2 amps to separate a pure fraction of non-magnetic materials.

4. Three fractions of different magnetic susceptibility are obtained: diamagnetic and paramagnetic minerals separated using the Frantz (Fig 3.5) and ferromagnetic minerals separated using neodymium magnets.

5. The three groups obtained are weighed, and the concentrations of these minerals in the initial sample are computed. The results are reported in Table 4.1.

6. Samples of diamagnetic material will be studied with optical and analytical techniques to identify the minerals further.

Figure 3.5: Example of the two separated fractions after the Frantz separator. The darker material is recognized as the magnetic part of the fraction, while the lighter material is due to its quartz concentration on a non-magnetic part.

3.2.4   Panning

The panning process consists of concentrating the heavy minerals using the drag of water and taking advantage of the difference in density of the Platinum and gold with respect to the other minerals in the sample. This technique is one of the oldest, most common, most efficient, and cheapest techniques for gold separation. However, for Platinum separation, it is one of the few, if not the only, way to extract Platinum sheets from sands [López-Males et al., 2020, Weiser and Schmidt-Thome, 1993].

Previous studies by Weiser & Schmidt-Thome (1993) reported that in the Santiago River areas, there is an occurrence of native Platinum and Pt-Fe alloys. This Platinum occurs in thin sheets that can be observed by microscopy. These heavy minerals suggest that the Santiago River is a possible source of these minerals of great economic interest. For this reason, panning was performed on the dark-type raw samples that were not used for granulometric and magnetic separation. The raw samples are used because, during the sieving process, the Platinum, presented in the form of flakes, could have remained in the sieves and lost during the following processes.

Procedure

For this washing and concentration of Platinum, a TurboPan acrylic pan and a 1.2 meter-long channel with a water flow of 0.2 to 0.3 liters per second were used, following the following process:

1. The heaviest or dark type samples are chosen because they have a higher concentration of heavy minerals, which are most likely to contain Platinum.

2. The channel is placed with an approximate inclination of 15°, and a constant water flow is connected at the upper end; the lower end is connected to a recovery container for the light material of the sample (Fig. 3.6a).

3. The sand is poured into the channel, starting at the top so that the drag of the water extracts the light particles and deposits the heavy particles within the channel grooves (Fig. 3.6b). As in magnetic separation, the amount of material entering and the speed of water entrainment must be controlled for uniform and efficient separation.

4. The material trapped in the channel grooves is carefully collected and passed to the pan (Fig. 3.6c). so that the heavy minerals are separated from the black sands with the help of the push of the water in a tidal effect (Fig. 3.6d).

5. Finally, the concentrate heavy material, gold, and Platinum are obtained, being the minerals of interest to be analyzed in the following steps.
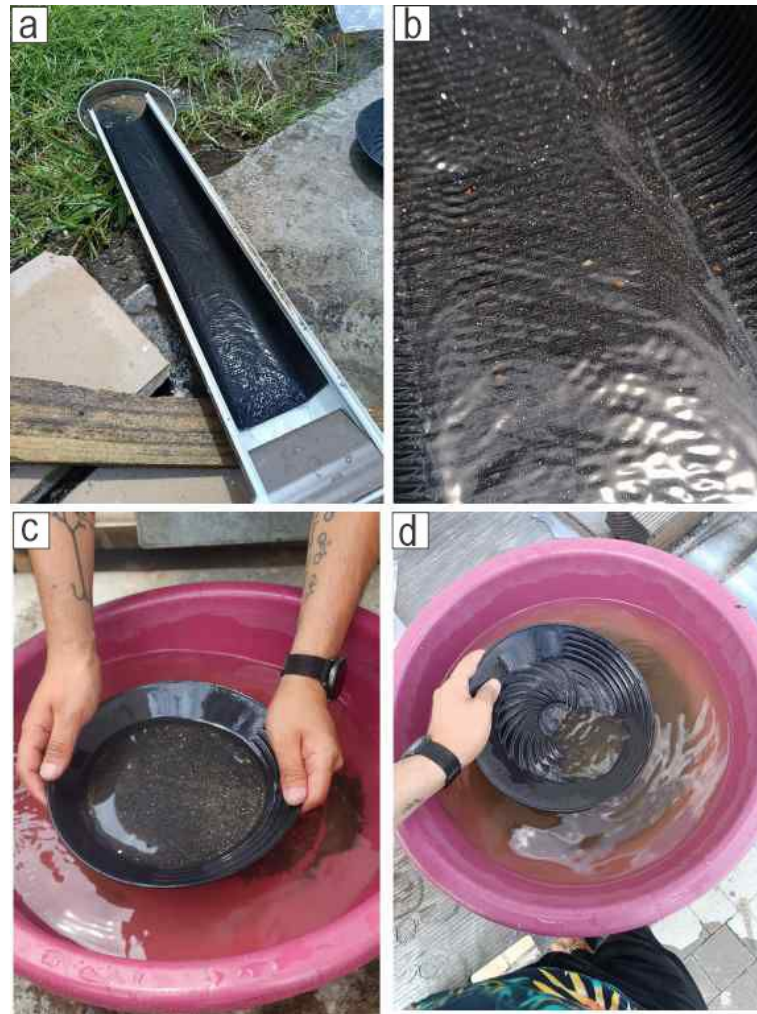
Figure 3.6: a) A separator channel or chute consists of a channel with deep spaces or grooves where the heavy minerals are trapped while dragged by the water, b) heavy mineral concentration in the chute's grooves, c) after passing the chute we put the material on a pan to continue the separation using the effect of gravity and water drag, d) concentrated and platinum-rich material left after panning.

3.3   Optical analysis of Minerals

In the previous sections, we used the physical properties of minerals to divide samples into smaller fractions. Various techniques involving measuring and recognizing physical parameters help us identify specific minerals. These grains with different compositions react to stimuli and exhibit specific characteristics that can be identified by looking at them directly [Klein et al., 2002].

According to Klein et al. (2002), the native characteristics of a mineral are its crystalline structure, hardness, color, and specific gravity. These unique characteristics can be identified in hand samples using basic field analysis instruments and the five senses. When this recognition is insufficient, or there is not enough evidence to affirm the presence of a mineral, samples are analyzed using more precise optical instruments. In this work, a qualitative analysis or descriptive mineralogy of the mineral grains was carried out to try to recognize most of them and how they are distributed in each of the separated fractions. Then, using instruments will help prove our guessing and identify the missing minerals with certainty.

3.3.1   Descriptive Mineralogy

The physical characteristics of minerals can be recognized with the naked eye in hand samples. In this way, each mineral presents its characteristics that researchers throughout history have described. In this way, authors such as Klein et al. (2002) have developed manuals for the recognition of the physical properties of most minerals, including crystal shape and crystal structure, luster, color, streak, cleavage, fracture, hardness, toughness, specific gravity, properties that depend on the configuration of light such as luminescence and fluorescence, and properties that depend on the electrical configuration of the material such as magnetism and radioactivity [Biswas et al., 2020]. This section describes the characteristics found in the minerals of the fractions separated during the magnetic separation stages (Ferromagnetic fraction, Paramagnetic fraction, and Diamagnetic Fraction) and the fraction corresponding to the concentration of heavy minerals by panning.

Equipment

For the recognition and description of the physical properties of the minerals, an Olympus SZX16 Stereomicroscope equipped with white light (Fig. 3.7), a long-wavelength ultraviolet light lamp (340 nm), an Olympus SC100 camera, and AnalySIS getIT software from Olympus Soft Imaging Solutions GmbH were used for recognizing minerals and capture images. A tungsten carbide-tipped pencil with a hardness between 8.5 and 9.5 on the MOHS scale was used to determine the hardness of the minerals.

Figure 3.7: Stereomicroscope Olympus SZX equipped with an SC100 camera in which we captured the high-resolution imagery of the mineral grains.

3.3.2 X-Ray Diffraction Analysis

In the previous section, we described the minerals we identified without using advanced optical analysis. Apart from the described minerals, there were other minerals of interest that descriptive mineralogy does not accurately describe. In consequence, the samples were submitted to an XRD test.

The sample preparation started by pulverizing the samples; once pulverized on a mortar, it was passed through a 450 MESH sieve, leaving us with a very fine powder to work with.

These powdered fractions will be mounted into disks and hit by Cu wavelength X-Rays, and the machine, based on the ray scattering produced by the crystalographic configuration of the minerals, will generate spectrographs to be analyzed later.

Equipment

A Benchtop Powder X-Ray Diffraction (XRD) Instrument was used. The Rigaku Corporation Miniflex X-Ray Diffractometer is a multipurpose equipment to get XRD from powders (Fig. 3.8a). The equipment can determine the crystalline phase and quantification, crystallinity percent, crystal size, lattice parameters, and molecular structure [Rigaku Corporation, 2023]. In this way, XRD analysis is widely used to determine the composition of a sample based on its crystalline configuration analysis. Once the spectrograph is generated, we must match the peaks with a certain mineral's correct model. We generated the percentages of the main mineral phases and elements using the software *Match!* and *QualX*.

The samples were analyzed, taking into account some parameters necessary to have the better resolution possible:

- The angles in which the XRD will be done are from 10º to 75º of sample inclination.

- The ferromagnetic and paramagnetic fraction samples were analyzed using an acrylic container because they could have been contaminated due to magnets in the metallic containers (Fig. 3.8b).

- The diamagnetic fraction samples were analyzed in the metallic containers without problem. In this case, the amount of powder was larger, as shown in Figure 3.8c.
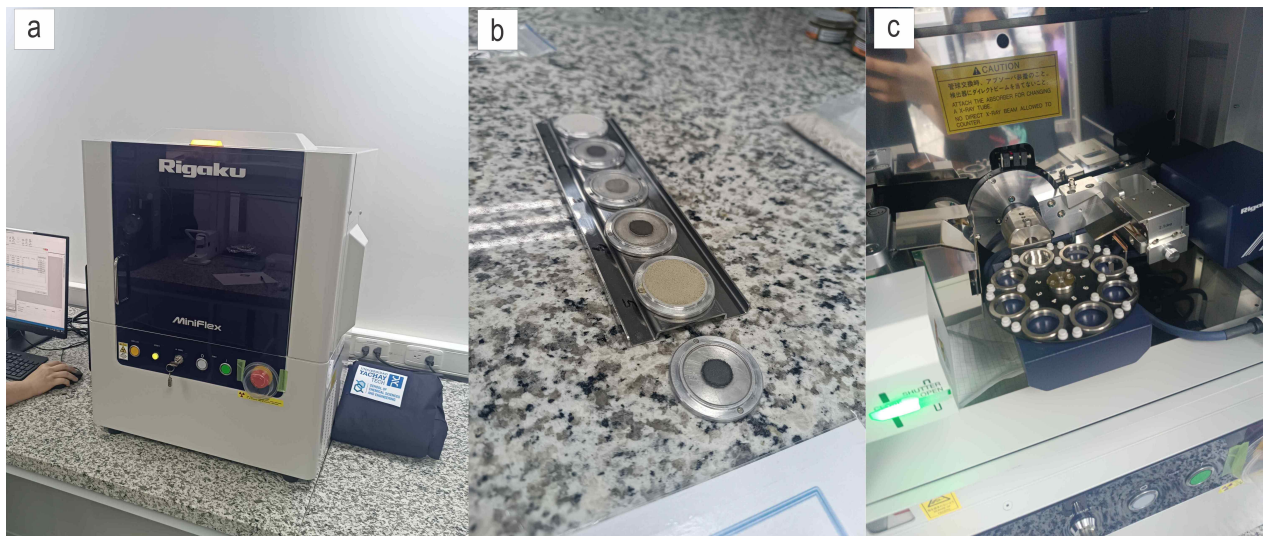
Figure 3.8: a) Miniflex XRD from Rigaku Corporation, the machinery which analyzed the minerals' crystallographic configuration. b) Sample preparation for the XRD analysis. We can observe the darker samples (ferromagnetic and paramagnetic) are contained in acrylic plates trying to avoid their potential interaction with the magnets in the metallic plates, while the lighter samples are contained in wider metallic plates. c) we can see eight spots to retain the samples inside the XRD machine. X-Rays will hit these samples at different angles. The machine will detect their diffraction rays and generate spectrograms that match precisely with some known materials so we can compare and find our minerals.

3.3.3 RAMAN Spectroscopy

In 1928 C.V. Raman and K.S. Krishnan discovered a *"New type of Secondary Radiation"* of light. The primary radiation is the one that corresponds to the usual state scattering of atoms and molecules [Andò and Garzanti, 2014]. While the secondary is described as the scattering of light in modified wavelengths that correspond to the fluctuation of the molecules from their normal state [Raman and Krishnan, 1928].

In this way, Raman spectroscopy is a useful, technological, and efficient tool to complement the analysis of minerals carried out in previous sections using a stereomicroscope [Andò and Garzanti, 2014]. The analysis can be done easily without complex sample preparation and, because it is a non-destructive technique, it can be used directly over the grains [Griffith, 1969]. This analysis can be used to fully identify some mineral grains that were not possible to describe under the microscope. Also, Raman spectroscopy eliminates operator error by analyzing deep into the crystal; it means we can see through the weathered, opaque, or contaminated surface layer to get a shot on a fresh mineral sample

[Andò and Garzanti, 2014]. Perhaps the most important fact of Raman examination is that it is a reliable study to determine heavy mineral grains just a few microns in size [Garzanti et al., 2011] that may have an oxidized or reworked surface; a task that is not possible with standard optical techniques [Andò and Garzanti, 2014].

Raman spectroscopy is a non-elastic light-scattering technique that analyzes the vibration of the molecules of a material which depends on its properties [Nasdala et al., 2004]. This technique is nowadays used to study economic ore deposits [Frezzotti et al., 2012, Jelenová et al., 2018].

According to Andò and Garzanti (2014), when monochromatic rays hit the molecules of a sample, usual elastic scattering occurs (light particles are scattered with the same energy and frequency), and only the 1×10^{-7} of the light is scattered with a different wavelength which is known as Raman radiation [Raman and Krishnan, 1928]. This small portion of photons released in a different wavelength gives information about the structural information we need.

In this way, we can apply Raman analysis to any mineral group [Andò and Garzanti, 2014], and it is based on identifying measured peaks that are similar or equal to reference spectra. The position of a peak on a determined spectrum is always the same for a mineral. Still, the intensity of the peaks will hardly depend on the crystal orientation, type of incident beam, and exposure time [Dietzek et al., 2018].

Equipment

A Horiba LabRAM HR Evolution RAMAN Spectrometer equipped with an OLYMPUS SC100 microscope, a 785nm laser, and a 25% ND filter. The acquisition parameters are: a range from 50 to 2000 cm^{-1}, 7s acquisition time, 7 accumulations, 3s of RTD time, a standard denoiser, and automatic laser mode.

Procedure

As seen in the previous section, Raman spectroscopy penetrates the crystals and analyzes their internal composition; such a thing is helpful in this work because we have reworked and altered grains whose surface is contaminated.

Using the microscope attached to the Raman Spectrometer, we can locate precisely the

grain and explore its surface to find a clear spot to shoot the laser. So, we analyzed the grains that could not be identified with basic optical analysis. Then, after the analysis, we have spectrums for each laser shoot.

- RRUFF Project

The RRUFF^{TM} project aims to create a big database of high-quality spectral data from well-characterized minerals. The project was created to have an easy way to analyze minerals in space exploration programs, such as interplanetary Rovers or space probes. Having an in situ Raman analyzer on the Special Purpose Vehicles (SPV) that goes to space, we can get real-time information on the rock samples instead of carrying them back here to analyze [RRUFF Project, 2016]. In this way, this database will improve the space career and also the further investigation of the Earth itself. RRUFF also provides software called *CrystalSleuth* to load the spectra and compares them with the online database.

3.3.4   X-Ray Photoelectron Spectroscopy: XPS

When light hits a material, some electrons are emitted; this is known as the photoelectric effect. According to this theory, electrons that materials emit are called Photoelectrons [Kloprogge and Wood, 2020]. The classical electromagnetic theory defines this effect as the energy transfer from the light to the electrons. Following this argument, the change in the intensity of the light may lead to a change in the kinetic energy of the electrons inside a material's atoms, which can be measured [Briggs, 2005].

The XPS analysis is not a penetrative test; it means that it just analyzes the surface of the material [Seyama et al., 2013]. The surface analysis came with careful preparation of the samples to avoid contamination [Mikhlin, 2020]. Therefore, XPS is a powerful tool for analyzing the effects of oxidation, abrasion, and alterations of the mineral grains.

According to Briggs (2005) and Kloprogge (2020), XPS analysis is based on irradiating solid materials with monoenergetic X-rays in a vacuum and recovering information about the number of photoelectrons emitted by measuring their energy. A plot is generated with the number of electrons per energy interval versus their kinetic energy [Mikhlin, 2020]. In this way, a unique spectrum is expected for each chemical element; then, in a mixture of elements, every peak for each element is detected [Briggs, 2005].

Equipment

A PHI 5000 VersaProbe III Photoelectron Spectrometer, equipped with a scanning electronic microscope (SEM) to locate the samples to shoot the laser at.

3.3.5 Inductively Coupled Plasma Spectroscopy - ICP

The Spectroscopic Multielement Analysis carried out by an ICP spectrometer is one of the fastest and most dominant tests nowadays because of its high precision measurements [Olesik, 2000].

The basic operation of an ICP is to use a partially ionized gas (commonly Argon, 1% ionized) shot from a quartz torch with a power supply that excites the atoms of the sample, which emit a characteristic and specific wavelength light that is detected and plotted [Olesik, 2000].

Some authors describe the ICP workflow as follows:

1. Sample preparation: The sample of interest is dissolved to create a homogeneous solution. This step ensures that the elements of interest are suitable for analysis [Moor et al., 2001].

2. The prepared sample is introduced into the ICP instrument, which converts the sample into a fine aerosol mist [Olesik, 2000]. The mist is then carried into the plasma torch.

3. The plasma torch consists of quartz tubes in which Argon gas is passed through and creates a gas flow. Energy is applied to a coil wrapped around the torch, inducing a magnetic field [Tyler and Yvon, 2003]. The magnetic field ionizes the argon gas, producing a high-temperature plasma beam [Chen et al., 2022].

4. As the sample mist enters the plasma flame, the high temperature causes the solvent to evaporate and leads atoms to excite to a higher energy level [Moor et al., 2001].

5. The excited atoms move to lower energy levels, emitting characteristic wavelengths of light. Each element emits specific wavelengths, forming a spectrum that is unique to that element [Olesik, 2000, Tyler and Yvon, 2003].

6. An optical system with lenses and mirrors collects the emitted light. A detector measures the intensity of the emitted light [Tyler and Yvon, 2003].

7. To determine the element concentration, a calibration curve is built using standard measurements. The measured light intensity is compared to the calibration curve, quantifying the atoms in the sample [Tyler and Yvon, 2003, Moor et al., 2001].

3.4 Point Counting Technique

Point counting is a reliable method to approximate the percentual composition of a sample. Many fields apply this technique, from analyzing biological samples to bacteria counting in medical research [Larrea et al., 2014] and even for estimation of birds population inside endangered or protected areas [Welsh, 2021].

The technique is also widely used in the analysis of geological samples. This way, minerals are counted in a sample to estimate compositions based on the type of minerals the researcher identifies. The most common samples to analyze in Earth Sciences are polished thin layers of rocks.

Researchers such as Larrea (2014) count the minerals in these thin sections. Because thin sections have a determined size, no matters how big the rock is, the number of points to count will always be statistically equal. It means if we have 30 minerals on a small thin section, all the thin sections from that rock will have approximately the same 30 minerals to count. As a result, the composition of the whole sample can be inferred based on the large amount of grains observed.

In searching for a perfect counting technique, some computational methods have been developed since the 90s. These methods have indeed made some difference, having new equipment that can be installed inside microscopes to help the identification [Catlin et al., 1992]. What the technology has improved is the accuracy of making equal grid divisions in the sample and having a unbias selection of the grid intersections.

For this work, we do not have any thin sections or professional and advanced equipment. Instead, we took photographs using the Stereomicroscope Olympus SZX16 equipped with an Olympus SC100 camera. In order to make it precise, we followed the following workflow:

1. From the fractions after the physical separation methods (Section 3.2), only the

diamagnetic fraction was taken into account for this analysis. The Ferromagnetic and Paramagnetic fractions were weighted, having their weight percentages right away.

2. For the Diamagnetic fractions, 5 grams of each sand was put inside a Petri dish.

3. From each Petri dish, 10 pictures were taken in different places and tried to have the same amount of grains in each run. Having more or less 80 minerals per picture, as we can observe in the example shown in Figure 3.9.
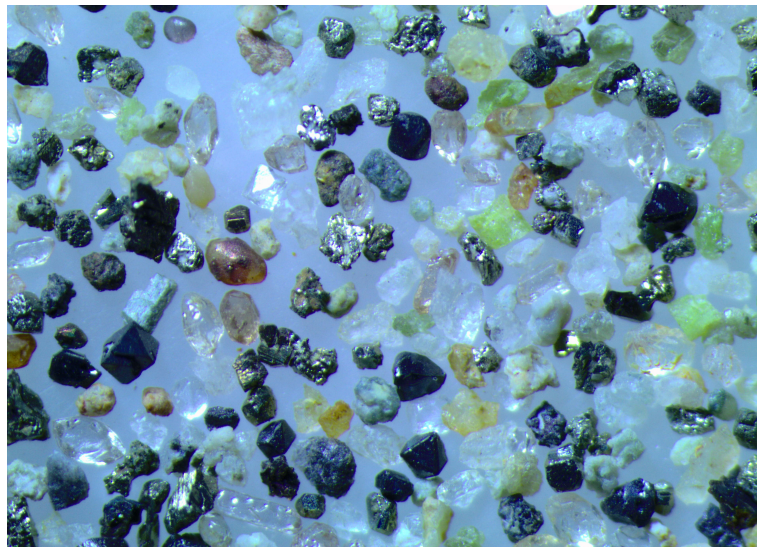
Figure 3.9: Picture taken with the Olympus SC100 camera. Sample PE-006, photo 9.

4. After having the photographs of the samples, we marked each mineral one by one using Inkscape software. The marks were counted for each different mineral having the final amount of grains per sample.

5. The data is plotted and interpreted, looking for the composition of the sand.

Chapter 4

Results

4.1 Sieving

The result of the sieving process is the representation of the weights of the fractions separated by the sieving machine. Values of the weight retained on each level are reported in Figure 4.1. Graphs show the major fraction of each sample; the blue column representing the 120 MESH sieve is generally the most abundant. Green highlighted values represent where the 80% of the whole mass passed; for the sample PE-001, 80 percent of the mass has passed the 18 MESH level, and the sample PE-004 has 80 percent of the mass passed the 60 MESH level; that data represents the d_{80} value.

	PE-001	PE-002	PE-003	PE-004	PE-005	PE-006	PE-007	PE-008	PE-009	PE-010
10 MESH	98.76	102.32	43.91	19.9	226.2	17.18	262.19	42.23	275.96	34.46
18 MESH	108.75	90.51	55.11	20.47	180.29	17.05	203.44	14.33	203.29	22.46
35 MESH	87.83	73.57	128.52	14.35	180.55	8.25	174.91	5.61	158.28	7.35
60 MESH	125.04	129.5	155.88	101.21	93.49	98.07	89.5	92.61	80.6	79.83
120 MESH	355.03	381.28	378.29	507.51	88.86	599.27	57.92	591.86	62.4	581.15
230 MESH	21.23	22.14	33.74	73.13	20.94	54.41	12.67	41.63	18.71	60.66
<230 MESH	3.42	3.08	6.11	5.18	12.34	2.09	7.13	2.07	8.65	4
TOTAL	800.06	802.4	801.56	741.75	802.67	796.32	807.76	790.34	807.89	789.91

Figure 4.1: Results from the granulometric separation in which the amount of material that passed through is represented in the graphs.

After Figure 4.1, it can be identified that the fractions that best represent the sample

and of which we have a larger quantity are those of 120 MESH. This information will allow us to focus on a single fraction per sample in the following analyses. In this way, it was decided to focus on the mineralogical characterization of all the fractions in samples PE-002, PE-004, and PE-006, and just the 120 MESH fraction in samples PE-001, PE-003, PE-005, PE-007, PE-008, PE-009, and PE-010.

4.2 Magnetic Separation

The resulting composition of the 10 samples that went through magnetic separation in the Frantz separator. They are classified into 3 main compositional groups: the ferromagnetic (fully magnetic) fraction was separated using neodymium magnets, the paramagnetic (induced magnetism) fraction using 0.3 to 0.8 amperes, and the diamagnetic (no magnetic) fraction. Results are presented in Table 4.1.

Table 4.1: Results on the percentage of the weight of each fraction after the magnetic separation.

	Ferromagnetic	Paramagnetic	Diamagnetic
PE-001	71.68%	15.98%	12.34%
PE-002	71.71%	15.99%	12.30%
PE-003	69.57%	15.51%	14.91%
PE-004	79.12%	17.64%	3.24%
PE-005	35.50%	7.91%	56.59%
PE-006	80.30%	17.90%	1.80%
PE-007	23.96%	5.34%	70.69%
PE-008	74.57%	16.62%	8.81%
PE-009	34.35%	7.66%	57.99%
PE-010	80.42%	17.93%	1.65%

4.3 Descriptive Mineralogy

From the panning process, we recovered one fraction of heavy-mineral concentrated sand. Then, as we saw in Table 4.1, the samples were magnetically separated into three fractions (Ferromagnetic, Paramagnetic, and Diamagnetic). In this section, we report the minerals we found in those fractions using the Stereomicroscope.

4.3.1 Ferromagnetic Fraction

The fraction extracted using a neodymium magnet in the magnetic separation stage was examined under the stereomicroscope, where Magnetite (Fe_3O_4) (Fig. 4.2) could be identified as the most abundant mineral. This mineral grain presents characteristics such as a greyish-black color, metallic luster, 6 (Mohs) hardness, an isometric crystal system, and a black streak.
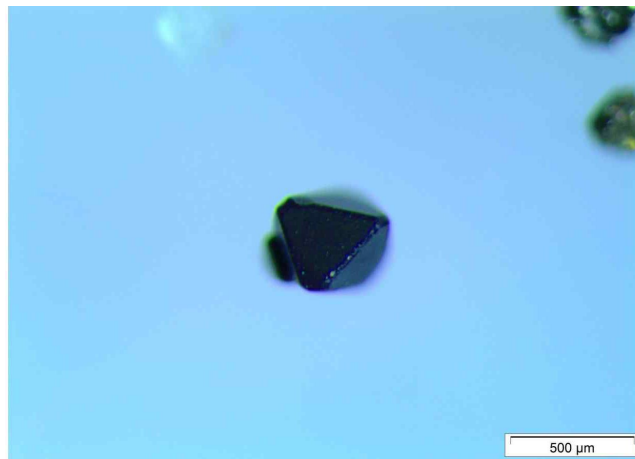
Figure 4.2: Magnetite crystals, the major component of the Ferromagnetic fraction of the samples.

4.3.2 Paramagnetic Fraction

The paramagnetic fraction was extracted during the magnetic separation stage using a magnetic field strength of 0.3 to 1.2 amps according to the protocol proposed by Londoño et al. (2010). Under the stereomicroscope, the most abundant mineral that could be identified was Ilmenite ($FeTiO_3$) (Fig. 4.3). The natural characteristics we found in the Ilmenite are the iron black coloration, metallic luster, 5-6 (Mohs) scale, a trigonal crystal system, and a reddish brown streak.
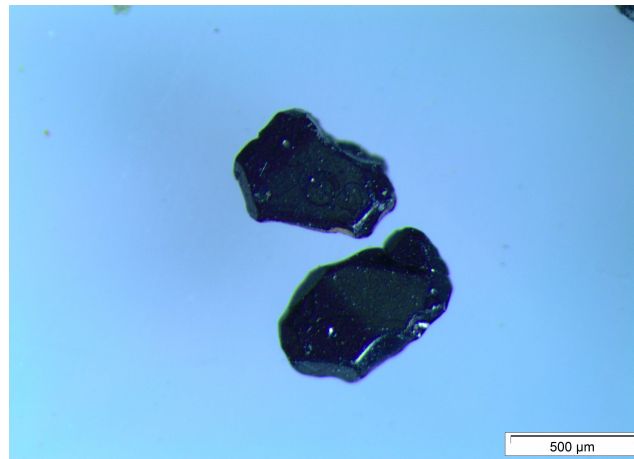
Figure 4.3: Ilmenite crystals, the major component of the paramagnetic fraction of the samples.

4.3.3   Diamagnetic Fraction

The diamagnetic fraction was separated by extracting all ferromagnetic and paramagnetic minerals, and this fraction is the most abundant in heavy minerals of interest. For the analysis of these sands and employing the Stereomicroscope, a description of the physical properties of each one of the minerals was made. The following minerals were identified with certainty:

Quartz (SiO_4)

The most abundant mineral within the non-magnetic or diamagnetic fraction is quartz, which has certain physical properties that are clearly distinguishable in Figure 4.4 as it is the yellowish-white, white and colorless color, vitreous to subvitreous luster, 7 Mohs hardness, and a trigonal crystal system.
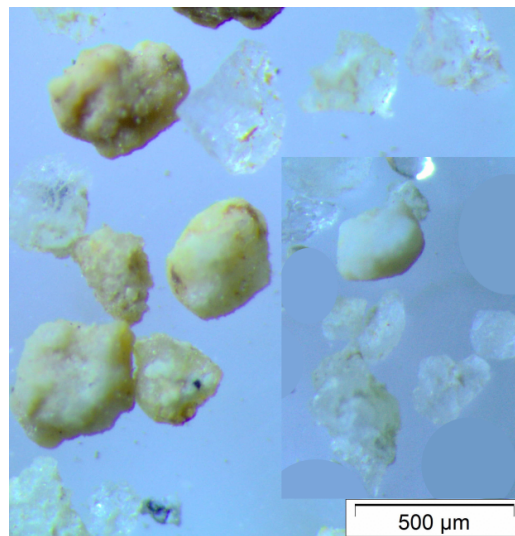
Figure 4.4: Quartz crystals from the samples.

Pyrite (FeS_2)

We recognized Pyrite as one of the most prominent iron sulfates in the samples. Its metallic luster and an isometric crystal system made it easy to recognize. In Figure 4.5, we can observe two different grain shapes: we have the cubic crystal, which is perfectly developed, while the other two show some alteration, deformation, and even polish due to the transport in the river.
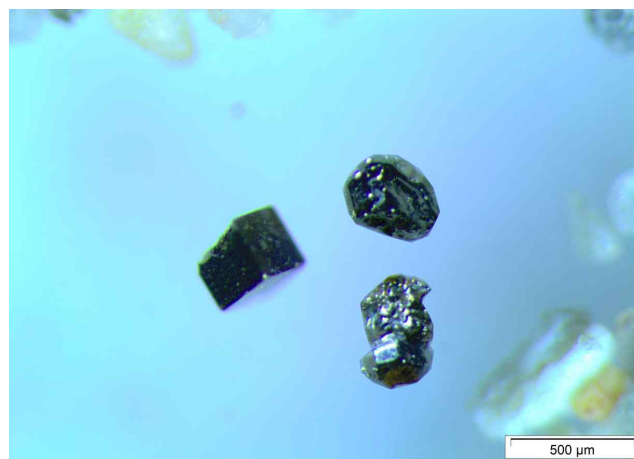
Figure 4.5: Pyrite crystals showing its classic cubic system.

Chalcopyrite ($CuFeS_2$)

We differentiate Chalcopyrite crystals from Pyrite mainly because of the presence of copper in the Chalcopyrite, which gives the crystal a yellowish-to-greenish color (Fig. 4.6. Also, it

was easy to determine that those crystals do not have an isometric crystal system, and they were easier to scratch, suggesting a minor hardness than Pyrite. We can observe in the figures that we have a tetragonal crystal system, and some yellowish colors are shown. All these characteristics are the clue to recognizing the Chalcopyrite crystals of the samples.
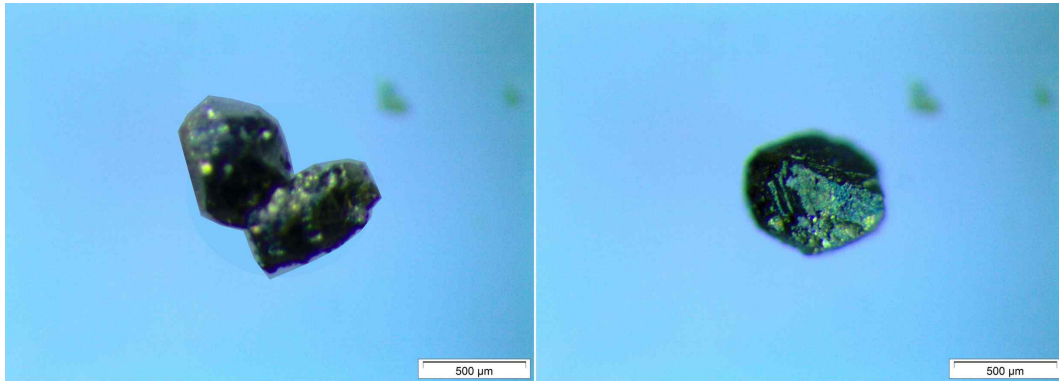
Figure 4.6: Chalcopyrite crystals where the greenish color is distinguishable.

Mercury Alloys

The exploitation of gold in Santiago River is closely related to illegality, and the use of Mercury as a gold collector is common. In this case, we found some mercury alloys in the samples. As we can observe in Figure 4.7 (red circle), these spheres of mercury were present among other crystals, and their perfectly round shape makes them easy to differentiate. In the laboratory, some of these spheres were separated to make some analysis to corroborate the presence of mercury. The spheres were heated with a Bunsen burner until the melting of the mercury was observed.
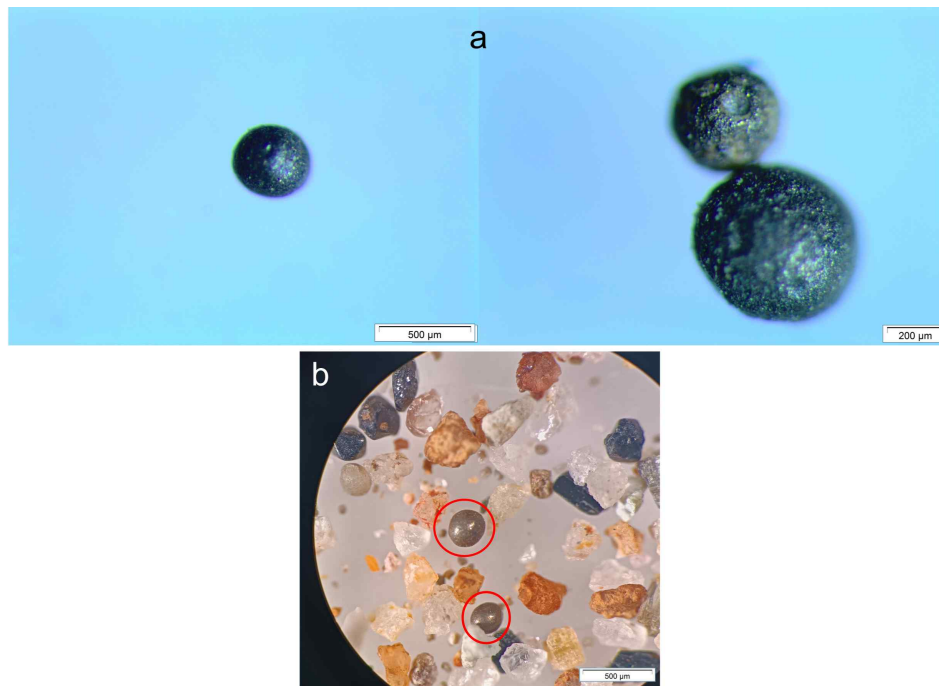
Figure 4.7: Mercury balls which are alloys with other metals.

Ferrosilite ($FeSiO_3$)

This iron silicate was observed and differentiated due to its orthorhombic crystals with dark brown to blackish colors and a distinguishable greasy luster (Fig. 4.8). In this case, this sample was also submitted to a Raman Spectroscopy analysis to define those crystals as Ferrosilite mineral grains accurately; the results of the Raman will be covered in the following sections.
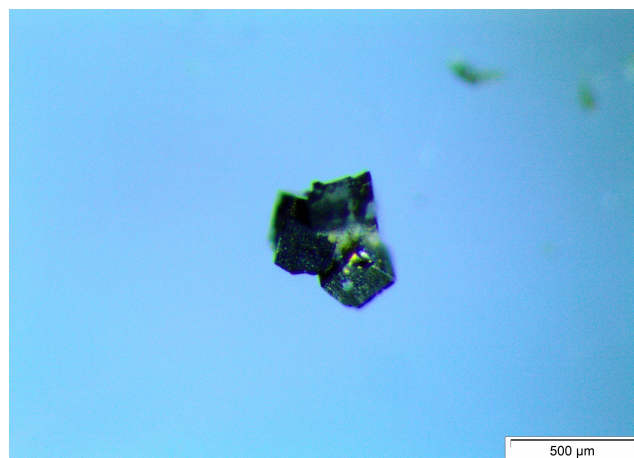
Figure 4.8: Ferrosilite crystals showing its orthorhombic and chaotic system.

Zircon ($ZrSiO_4$)

The presence of Zircon grains was revealed using Ultraviolet light with a long wavelength of 340nm. Zircon crystals exposed to long wavelength UV lights show fluorescence in orange or yellow colors [Mineralia.org, 2015]. As we can see in Figure 4.9c: the zircon crystals are shining in orange and yellow colors; the color difference may be related to a certain degree of alteration [Bevandić et al., 2021]. The alterations are visible under the stereomicroscope and have differences, as seen in Figure 4.9. We see a zircon grain (Fig. 4.9b) that had been broken apart and polished until having that rounded grain (Fig. 4.9a); it shows a yellowish fluorescence (Fig. 4.9c).
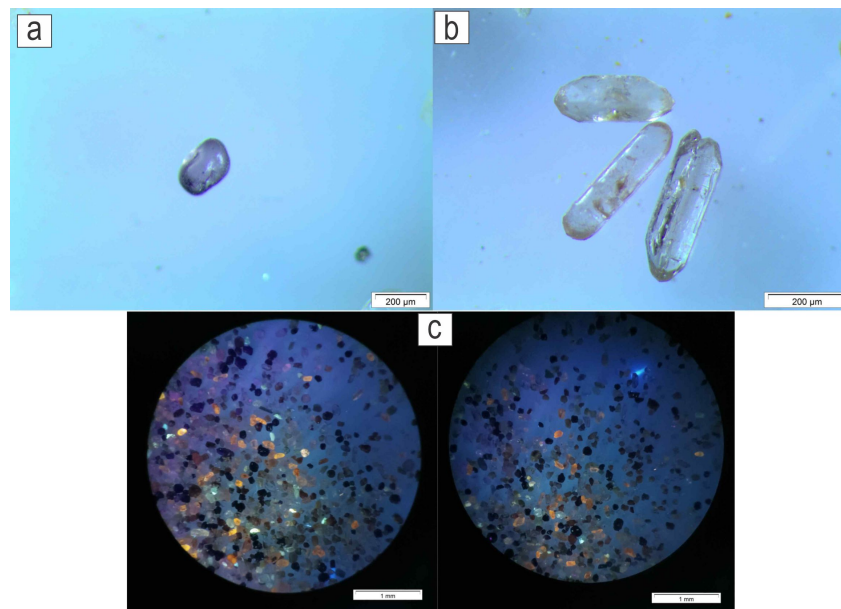
Figure 4.9: Zircon grains fresh (b), altered (a), and under UV light (c).

Fluorite (CaF_2)

Mineralia.org (2015) fluorescence tables report Fluorite to show a blueish fluorescence when exposed to long wavelength UV light (Fig. 4.10b). Using this principle, we identified fluorite crystals in the samples. They are pale yellow and show alterations related to graining, as shown in Figure 4.10a.
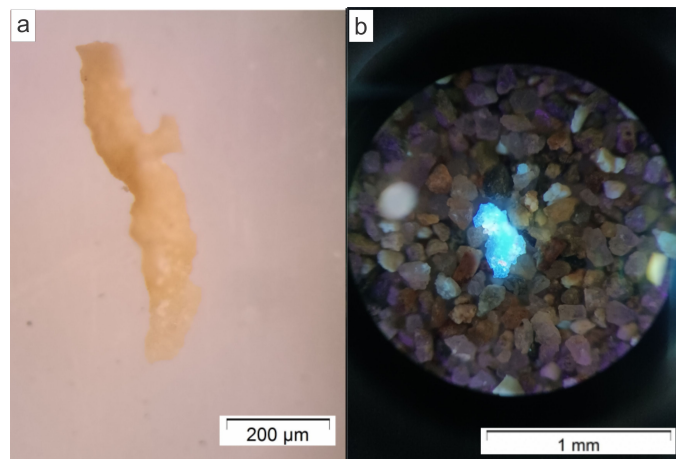
Figure 4.10: Fluorite grains which show orange to yellow colors (a) and blue fluorescence (b).

4.3.4 Heavy Mineral Fraction

This fraction was extracted by passing the material through a chute which retains the material in its grooves and then is concentrated by panning. We ended up with a heavy fraction containing two minerals of interest:

Gold (Au)

Recognizing gold is relatively easy when we have a few heavy minerals of interest on river sands [Techera and Arrighetti, 2002]. The classic rich yellow color, metallic luster, and low (2-3 Mohs) hardness make it easy to determine it was gold. They are present in flakes and grains with sizes from 500μm to 2mm, which the previous mining processes did not extract (Fig. 4.11).
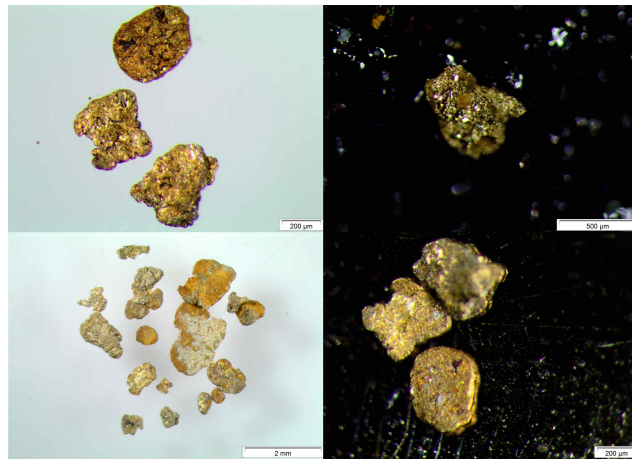
Figure 4.11: Gold flakes found in the heavy concentrated, which show the classic yellowish golden color.

Platinum (*Pt*)

One of the heavy minerals with high interest in this work is platinum. These mineral flakes are present in the fraction concentrated by panning (Fig. 4.12). It has a steel grey color, metallic luster, and low hardness (3-4 Mohs). This mineral will be further analyzed with other techniques to get further information about its mineralogy [Yakubovich et al., 2023].
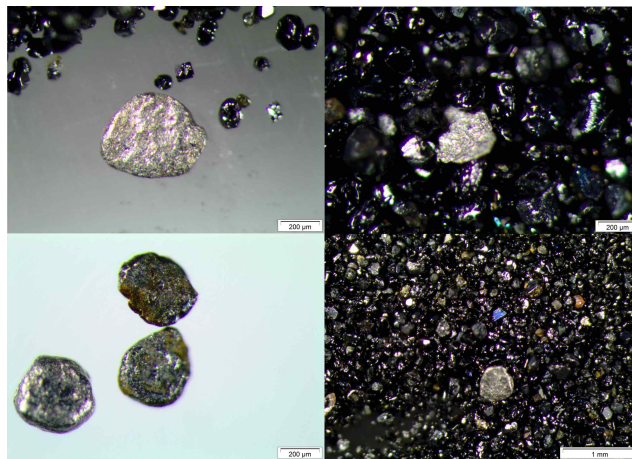
Figure 4.12: Platinum flakes are difficult to find but easily recognizable by their color and luster.

4.4   X-Ray Diffraction (XRD)

For this analysis, we picked samples from each group: the ferromagnetic fraction, the paramagnetic fraction, and the diamagnetic fraction having the following results:

4.4.1   Ferromagnetic Fraction

Phases and elements found by the XRD analysis ran in the ferromagnetic sample. We can distinguish two main mineral compositions: Magnetite and Ilmenite, and the presence of three main elements Iron, Titanium, and Oxygen (Fig. 4.13).
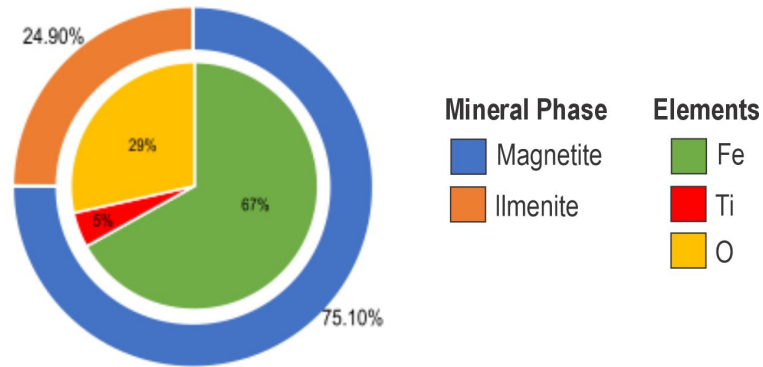
Figure 4.13: Ferromagnetic fraction composition after the XRD analysis.

4.4.2   Paramagnetic Fraction

Phases and elements found by the XRD analysis ran in the paramagnetic sample. In this case, the analysis recognized just one mineral: Ilmenite, reported as 100% of the composition, and the presence of three main elements: Iron, Titanium, and Oxygen (Fig. 4.14).
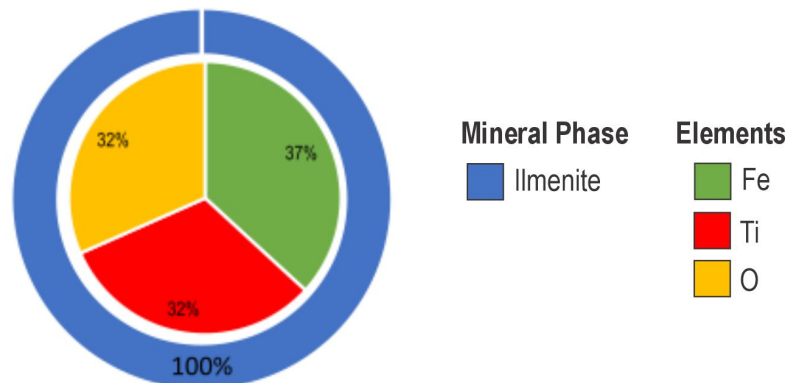
Figure 4.14: Paramagnetic fraction composition after the XRD analysis.

4.4.3   Diamagnetic Fraction

Phases and elements found by the XRD analysis ran in the diamagnetic sample. In this analysis, we surprisingly found just two minerals: Quartz and Zircon, and the presence of

three main elements: Silica, Zircon, and Oxygen (Fig. 4.15).
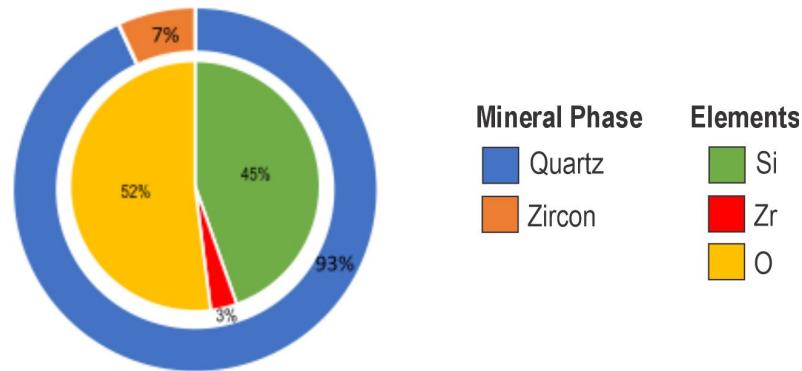
Figure 4.15: Diamagnetic fraction composition after the XRD analysis.

4.5   RAMAN Spectroscopy

1.   For this work, we wanted to analyze the grains we could not identify in Sections 3.3.1 and 3.3.2. To do that, we picked up the best grain to explore its surface until finding the perfect spot where the laser hit. Then we did 3 shots per grain, two grains per mineral, having the following minerals encountered:

Brucite ($Mg(OH)_2$)

Unknowk grains were analyzed using RAMAN spectrometry in the laboratory; the resulting spectrum is shown in Figure 4.16a, where we can see a clear peak around 400 cm^{-1} This peak coincides with the peaks reflected in the RRUFF database spectra shown in Figure 4.16b. The noise is related to the impurity of the samples [Haskin et al., 1997].

Also, an image of Brucite grain is reported in Figure 4.16, in which we can observe some characteristics such as its waxy to pearly luster and hardness around 2.5 Mohs. Brucite grains are easy to break using the tungsten carbide pen. They also show some alteration and weathering.
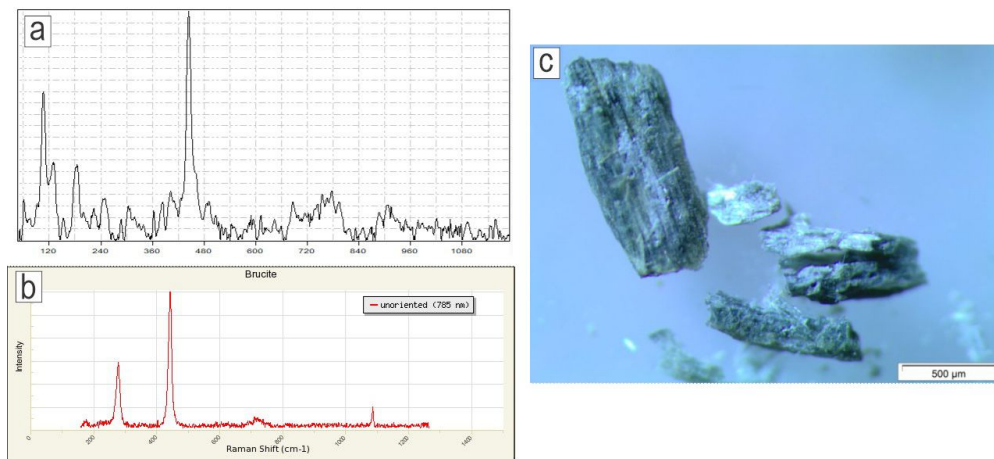
Figure 4.16: Brucite crystals recognized after RAMAN spectroscopy (c). Laboratory spectrum (a) and RRUFF database spectrum (b).

Annite ($KFe_3AlSi_3O_{10}(OH, F)_2$)

Annite mineral grains were recognized using the RAMAN spectra (Fig. 4.17a) recovered at the laboratory and the CrystalSleuth software, having an 89% match with the mineral *Annite*. This phyllosilicate mineral belongs to the Biotite group of the Mica family [Mineralia.org, 2015]. It is a soft mineral (3 Mohs) with vitreous luster and shows some transparency in its monoclinic crystal system, as we can observe in Figures 4.17b and c.
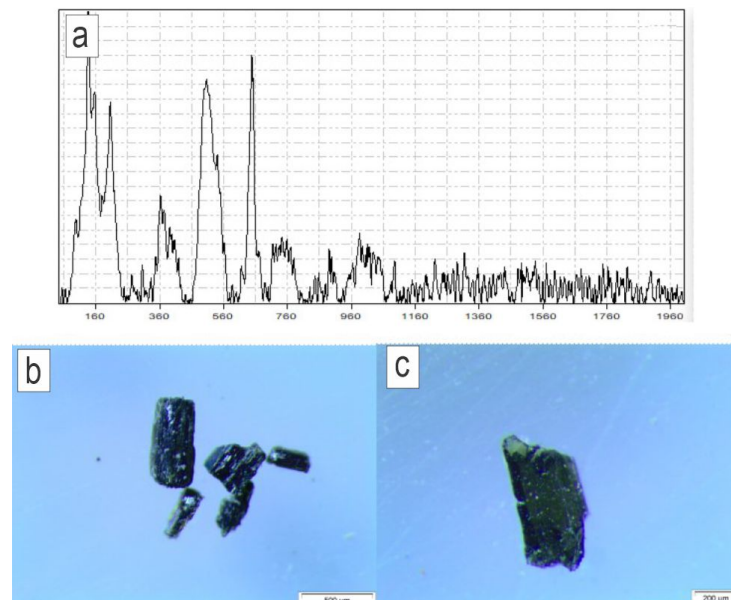
Figure 4.17: Annite spectrum after the RAMAN spectroscopy (a), and some crystals observed under the microscope in which we can differentiate some physical characteristics (b,c).

Berlinite ($AlPO_4$)

This rare high-temperature hydrothermal or metasomatic mineral belongs to the phosphates family [Mineralia.org, 2015]. In Figure 4.18a, we can see a RAMAN spectrum for the transparent crystals first identified as Quartz, which are now described as *Berlinite*. We can compare with Figure 4.18b (RRUFF Database spectra), where the peaks around 400 and 1100 cm^{-1} match almost perfectly. CrystalSleuth gives a 94% match for those two spectra. In Figure 4.18c, it can be observed that the crystals are transparent, vitreous in luster, and with hardness like Quartz (6.5 Mohs).
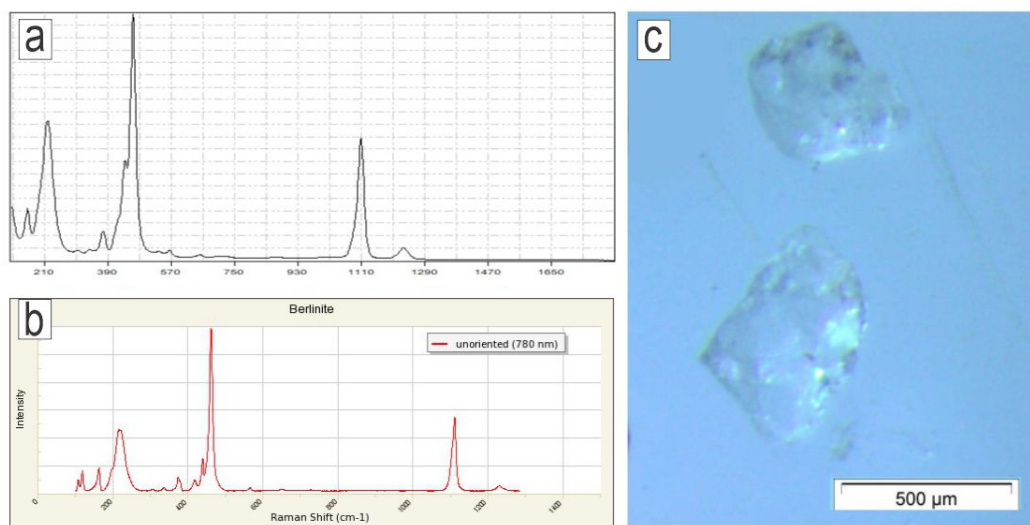
Figure 4.18: Berlinite spectrum after RAMAN spectroscopy: a) measured spectra, b) RRUFF database spectra, and c)crystals of berlinite under the microscope.

Epidote ($Ca_2FeAl_2(Si_2O_7)(SiO_4)O(OH)$)

Epidote mineral is characterized by being a product of hydrothermal alteration of various igneous rock-forming minerals [Mineralia.org, 2015]. In Figure 4.19a, a RAMAN spectrum gathered at the laboratory shows peaks around 900 cm^{-1} that coincide with the peaks in Figure 4.19b, which is an RRUFF database spectrum. The CrystalSleuth Software gives a 78% match for *Epidote*. This mineral, characterized by its vitreous luster and monoclinic crystal system, is present in the samples as yellowish-green color grains (Figure 4.19c).
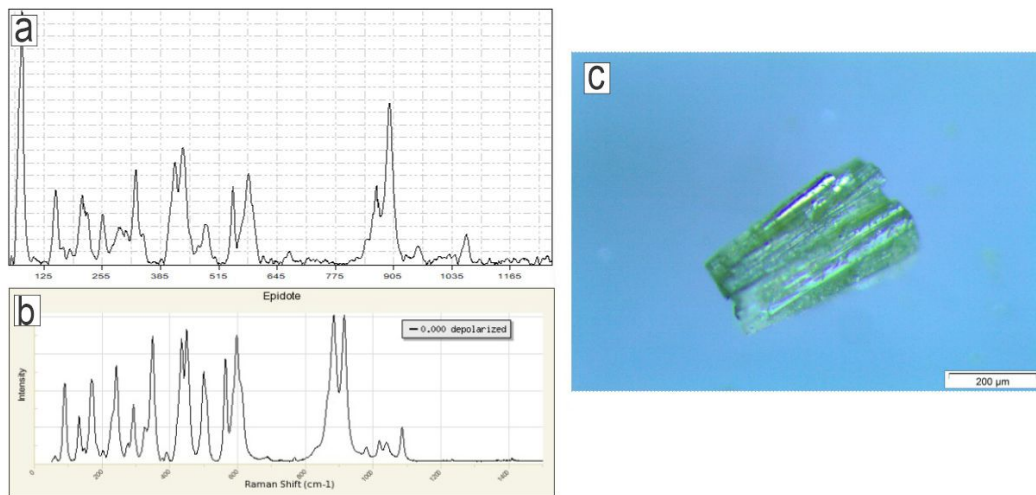
Figure 4.19: Epidote spectra are shown in **a** (measured) and **b** (RRUFF database). **c** shows an epidote crystal under the microscope.

2. Some minerals were also analyzed using RAMAN Spectroscopy with the objective of double-checking the identification carried out in Section 3.3.1. In this way, some minerals were analyzed using the same technique. The results corroborate the first assumption, and the following spectrums were gathered:

Ferrosilite ($FeSiO_3$)

After checking the ferrosilite crystals, a spectrum was generated and it was compared with the RRUFF database spectrum in Figure 4.20. CrystalSleuth software reported an 80% of coincidence with *Ferrosilite* mineral.
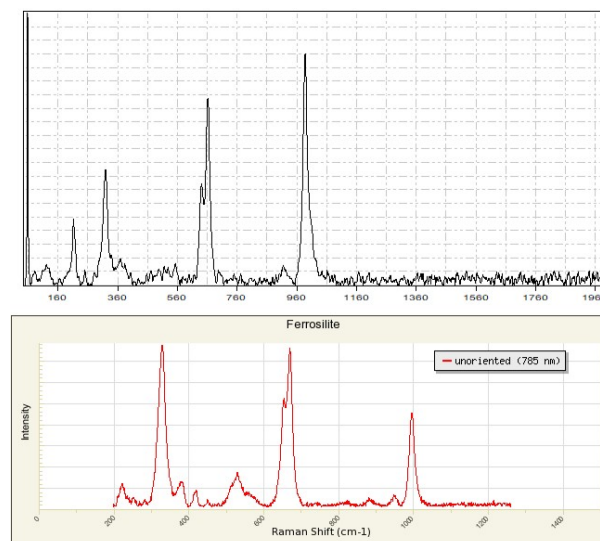
Figure 4.20: Ferrosilite RAMAN Spectrum comparison.

Zircon ($ZrSiO_4$)

For the Zircon mineral, we wanted to find similarities to corroborate our findings, so we have Figure 4.21 with the measured spectrum at the top and at the bottom the RRUFF database spectrum, which has a 93% match with *Zircon* according to the CrystalSleuth software.
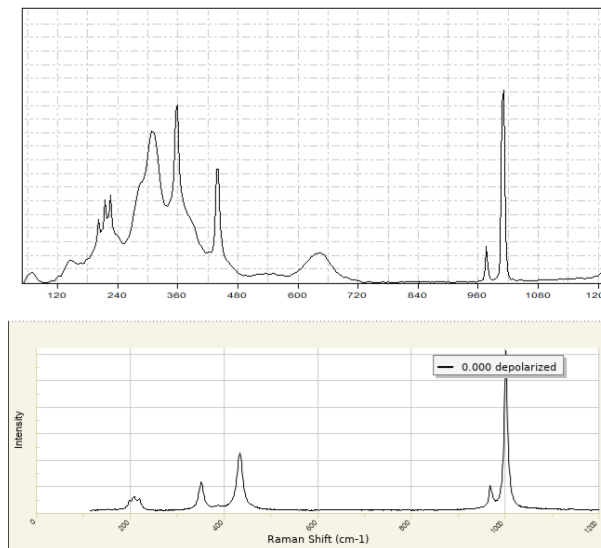
Figure 4.21: Zircon RAMAN Spectrum comparison.

Gold (Au)

The main objective of analyzing gold with Raman spectroscopy is to, in a certain way, look at the purity of the sample [Griffith, 1969]. In Figure 4.22, we can see the top representing our measured spectra, and the bottom is the RRUFF project spectrum. According to Griffith (1969) and Haskin et al. (1997), the noise is related to the purity of the sample; in other words, more noise means alteration and weathering of the mineral grain.
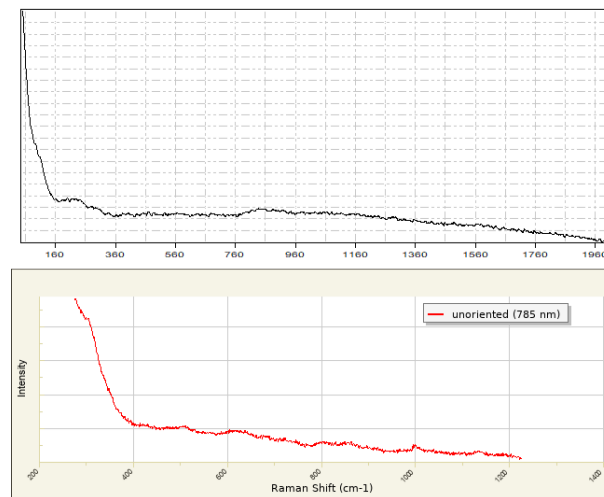
Figure 4.22: Comparison of Raman spectrum of Gold grains.

Pyrite (FeS_2)

We can observe in Figure 4.23, that the top represents the measured RAMAN spectrum which, compared to the RRUFF database at the bottom, CrystalSleuth found 94% of matching with *Pyrite*.
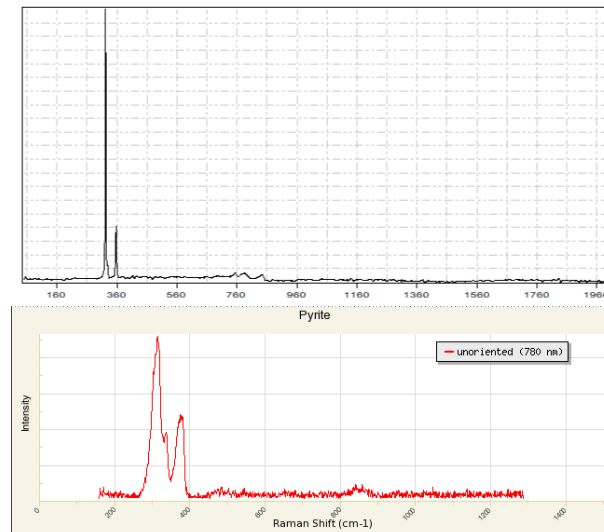
Figure 4.23: Comparison of RAMAN Spectrum for Pyrite.

Magnetite (Fe_3O_4)

The perfect Magnetite crystals of Figure 4.2 were analyzed. When comparing both spectra in Figure 4.24 (top-measured, bottom-RRUFF), CrystalSleuth finds an 84% matching, corresponding to *Magnetite*
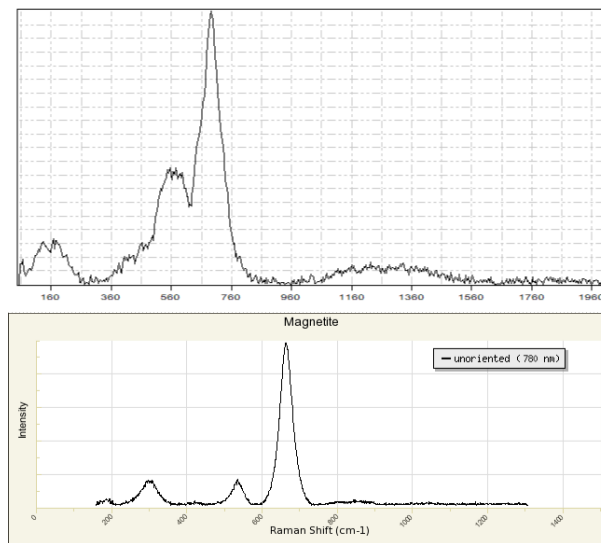
Figure 4.24: Comparison of Magnetite RAMAN Spectrum.

Ilmenite ($FeTiO_3$)

The ilmenite crystals were also analyzed and compared using CrystalSleuth. Figure 4.25 show the measured spectrum on top and the RRUFF database spectrum at the bottom. Both of them have an 89% coincidence, corresponding to *Ilmenite.*
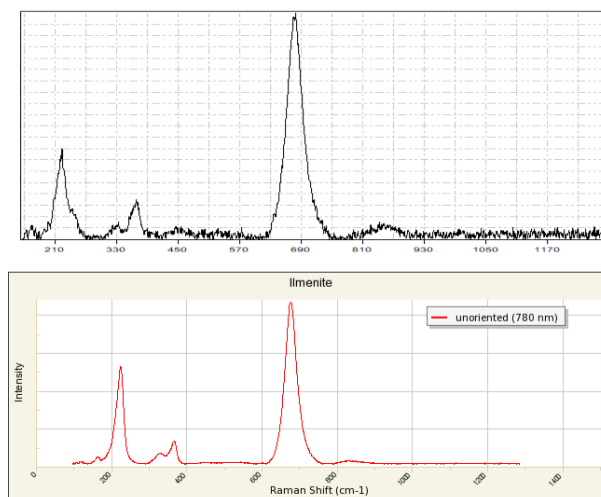
Figure 4.25: Comparison of Ilmenite RAMAN Spectrum.

Platinum (Pt)

As it is of major interest, Platinum flakes were also analyzed using Raman spectroscopy. In Figure 4.26, the top figure represents the measured spectrum, and the bottom represents

the RRUFF database spectrum. Some interesting peaks are found at 260 cm^{-1}, and the matching that CrystalSleuth reports is 87% with *Platinum.*
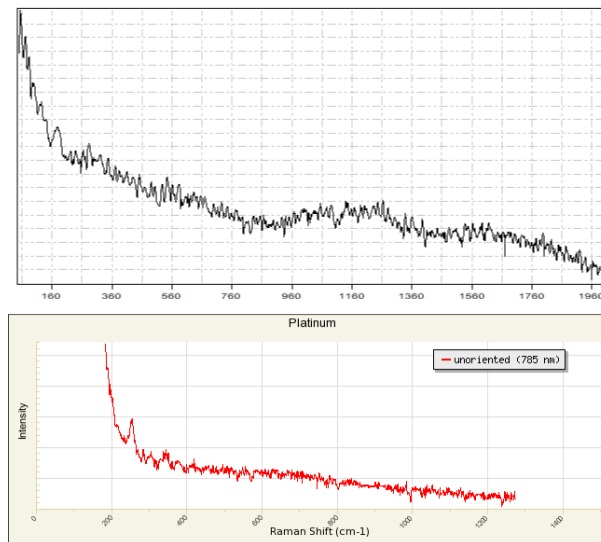
Figure 4.26: Comparison between Platinum RAMAN spectrum.

4.6 XPS

The XPS analysis is the most time-consuming because of sample preparation, it must be very carefully done. Hence, we analyzed some minerals to corroborate the findings in Sections 3.3.1, 3.3.2, and 3.3.3. The following spectrums with their chemical composition were found:

Epidote ($Ca_2FeAl_2(Si_2O_7)(SiO_4)O(OH)$)

The mineral grain surface is analyzed using XPS, and the peaks are reported in Figure 4.27 with the red line. Each peak corresponds to a certain chemical element. The atomic percentage is also reported to have Oxygen as the major compound, then Cl, Si, Al, Mg, N, Ca, and Fe. Those measurements match the chemical composition of Epidote reported by Mineralia.org (2023): $Ca_2Fe^{3+}Al_2(Si_2O_7)(SiO_4)O(OH)$. Having Mg as a contaminant element in the sample.
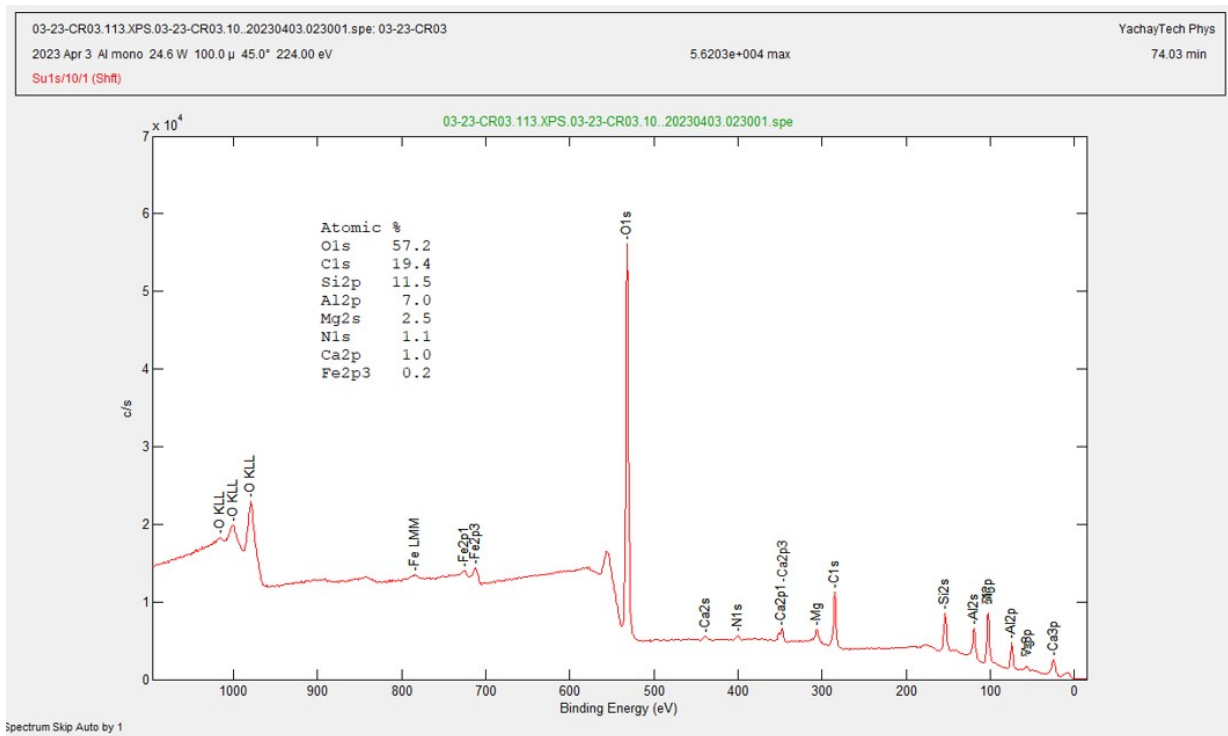
Figure 4.27: XPS analysis for Epidote crystals where its chemical composition is shown.

Fluorite (CaF_2)

The double check for the Fluorite left us with Figure 4.28 in which we can observe a high Oxygen and Carbon content, probably because of contamination while handling the samples. The following elements are for sure contaminants, oxidants, or other alterations in the mineral. We have the expected Fluor and Calcium in fewer quantities that match the chemical formula of Fluorite: CaF_2.
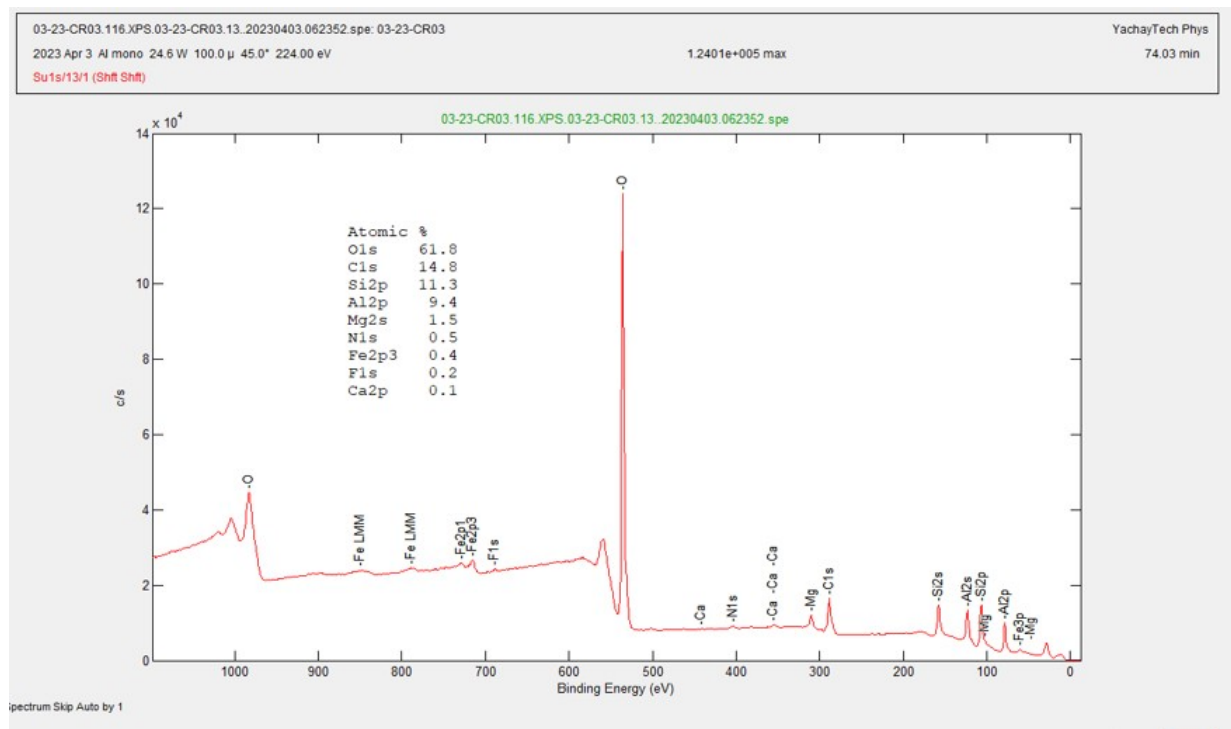
Figure 4.28: XPS spectra for Fluorite grains in which we can observe their chemical composition.

4.7   ICP

"For this work, the ICP analysis was carried out at the University of Granada in Spain by Doctor Fernando Gervilla and his team, to whom we express our sincere gratitude.

Two tests were performed: an ICP-OES and an ICP-MS of a heavy mineral-rich sample, having the following findings:

4.7.1   Inductively Coupled Plasma Optical Emission Spectroscopy: ICP-OES

For the ICP-OES test, we have the results of the analysis for major element concentration in a raw sample. Table 4.2 contains the results of a test performed on a heavy mineral-rich sample using the ICP-OES test. The chemical composition of each major element is reported, being the Iron the major component of the sample.

Table 4.2: Results of ICP-OES analysis for major elements.

Major Elements	Weight %
Al	0.4409
Ca	0.2167
Fe	54.9
K	0.0085
Mg	0.4972
Na	0.0126
S	1.645

4.7.2   Inductively Coupled Plasma Mass Spectroscopy: ICP-MS

For the ICP-MS test, the sample is analyzed looking for minor elements and trace elements.

Minor Elements

Minor elements concentration in the sample is shown in Table 4.3; we have Titanium as the major occurrence. These Minor elements are reported in PPM (parts per million) and transformed into weight percent.

Table 4.3: Minor elements results after an ICP-MS analysis.

Minor elements	Ppm	Weight %
Ti	1.11E+05	11.144055
Ru	0.003	0.0000003
Pd	0.028	0.0000028
Ag	0.169	0.0000169
Re	0.004	0.0000004
Ir	0.08	0.000008
Pt	2.678	0.0002678
Au	0.584	0.0000584

Trace Elements

Table 4.4 represents the concentration of trace elements found in the sample. They are reported in PPM and transformed into weight percent. The following table reports the amount of REE encountered and other elements that are present in the samples accompanying the REE.

Table 4.4: ICP-MS analysis results for trace elements in the sample.

Trace Element	Li	Rb	Cs	Be	Sr	Ba
Ppm	1.01	0.29	0.1	0.13	15.93	11.37
Weight %	0.000101	0.000029	0.00001	0.000013	0.001593	0.001137
Trace Element	Sc	V	Cr	Co	Ni	Cu
Ppm	26.73	2438.09	542.56	149.08	47.24	90.85
Weight %	0.002673	0.243809	0.054256	0.014908	0.004724	0.009085
Trace Element	Zn	Ga	Y	Nb	Ta	Zr
Ppm	299.86	20.65	3.62	43.6	2.6	137.04
Weight %	0.029986	0.002065	0.000362	0.00436	0.00026	0.013704
Trace Element	Hf	Mo	Sn	Tl	Pb	U
Ppm	4.04	3.34	9.61	0.06	7.59	0.42
Weight %	0.000404	0.000334	0.000961	0.000006	0.000759	0.000042
Trace Element	Th	La	Ce	Pr	Nd	Sm
Ppm	1.03	3.53	12.26	0.88	3.84	0.77
Weight %	0.000103	0.000353	0.001226	0.000088	0.000384	0.000077
Trace Element	Eu	Gd	Tb	Dy	Ho	Er
Ppm	0.31	0.8	0.1	0.66	0.15	0.55
Weight %	0.000031	0.00008	0.00001	0.000066	0.000015	0.000055
Trace Element	Tm	Yb	Lu			
Ppm	0.1	0.63	0.09			
Weight %	0.00001	0.000063	0.000009			

These values are compared with the concentration of elements in Earth's crust to see which one has a greater concentration than expected and which may be considered an anomaly. Table 4.5 shows the so-called anomalies found for the trace elements in yellow. The anomalies are determined as elements with a higher concentration than the earth's crust and may be of possible interest for future exploration.

Table 4.5: ICP-MS analysis results comparison of trace elements with the normal abundance in the crust. Values reported in PPM.

Element	Crust Average	Test	Element	Crust Average	Test
Li	18.50	1.01	Ga	18.50	20.65
Rb	150.00	0.29	Y	29.50	3.62
Cs	2.45	0.10	Nb	18.50	43.60
Be	2.25	0.13	Ta	1.85	2.60
Sr	365.00	15.93	Zr	190.00	137.04
Ba	420.00	11.37	Hf	4.30	4.04
Sc	21.00	26.73	Mo	1.30	3.34
V	150.00	2438.09	Sn	1.47	9.61
Cr	172.50	542.56	Tl	0.57	0.06
Co	25.00	149.08	Pb	12.00	7.59
Ni	120.00	47.24	U	0.90	0.42
Cu	72.67	90.85	Th	9.00	1.03
Zn	77.00	299.86			

In the same way, the REEs were compared to know which elements are present in greater quantities than in the earth's crust. In this way, it is identified that none of the elements have high concentrations that could suggest a possible source of exploitation in the areas of the Santiago River; the results are reported in Table 4.6.

Table 4.6: REE compared with the abundance in Earth's crust. Values reported in PPM.

REE	Crust Average	Test
La	38.27	3.53
Ce	78.13	12.26
Pr	8.90	0.88
Nd	35.23	3.84
Sm	6.23	0.77
Eu	1.26	0.31
Gd	4.88	0.80
Tb	0.87	0.10
Dy	5.10	0.66
Ho	1.06	0.15
Er	3.16	0.55
Tm	0.48	0.10
Yb	2.98	0.63
Lu	0.50	0.09

4.8   Point Counting

For this work, first, we calculated the percentage of Magnetite and Ilmenite we have on each 10 pictures from each of the 10 samples that were taken. So, we have to count approximately 70 minerals from each picture, having an average of 700 grains per sample, giving a total of 6925 mineral grains counted.

From Section 3.2.3. we got the weights of the separated Diamagnetic, Paramagnetic, and Ferromagnetic fractions, which left us with a Table 4.7 that reports the average percentage from the 10 samples.

Table 4.7: Percentual compositions of each of the fractions after magnetic separation (Section 3.2.3).

Ferromagnetic	70.95%
Paramagnetic	16.19%
Diamagnetic	12.86%

The ferromagnetic fraction is composed mainly of Magnetite and the Diamagnetic fraction of Ilmenite, as shown in Figures 4.13 and 4.14. From Table 4.7, we must do the following division of the Diamagnetic fraction. That is, the 12.86% divided into 13 other mineral proportions.

In the end, this work has identified 15 minerals in the samples. The final mineral composition of the 10 samples analyzed is reported in Table 4.8:

Table 4.8: Final results for the mineral composition of the samples from Santiago River.

a			b	
Mineral	**wt %**		**Mineral**	**wt %**
Magnetite	70.95%		Quartz	60.59%
Ilmenite	16.19%		Brucite	8.03%
Diamagnetic	12.86%		Zircon	6.47%
			Annite	6.33%
			Pyrite	5.92%
			Berlinite	3.65%
			Epidote	3.20%
			Fluorite	2.90%
			Chalcopyrite	1.34%
			Ferrosilite	0.80%
			Mercury	0.44%
			Gold	0.31%
			Platinum	0.00%

Chapter 5

Discussion

The alluvial deposits along the Santiago River in the province of Esmeraldas, being of high economic value due to the presence of gold, make the composition analysis necessary. This work has tried, through the use of classic and modern techniques, to give an idea of how the auriferous sands and gravels of the north coast region are composed.

Londoño (2010) and Rosenblum and Brownfield (1999) present a protocol for analyzing samples for mineralogical characterization. In this way, the analysis begins with the realization of a physical separation that helps us to divide the work into smaller portions and then proceed with a more exhaustive study of the obtained fractions.

The drying of the samples is fundamental for the realization of the granulometric separation due to the fact that only a gravity separator is available. In spite of the fact that the bibliography recommends making a separation that uses the push of the water. The test was carried out successfully for the 10 samples, the objective of which was to find the grain size arrangement of each fraction. Thus, the result presented in Figure 4.1 was obtained, where the value corresponding to the sieve that allowed 80% of the material to pass (d_{80} value) can be seen in green. Finally, the fraction that best represents the sample is obtained, this being the 120 MESH grain size fraction.

The fractions of 120 MESH (0.025 - 0.125 mm) that were obtained with the granulometric separation are the fractions that passed through the following characterization stages. In this way, the magnetic separation was done, and the results, represented in Table 4.1, were good for determining the content of Magnetite and Ilmenite in the samples, as reported in Table 4.8 Where it can be observed that 70% of the material is Magnetite. Commonly,

magnetite is the main component of the so-called "black sands" [Jamieson et al., 2015]. As these samples are taken from artisanal mining tailings, they are expected to have a high content of this heavier fraction. In fact, magnetite is part of the heavy material remaining after gold mining [Jelenová et al., 2018]. This material may be of interest due to its high percentage of iron, as seen in Figure 4.13. On the other hand, Ilmenite, the main component of the Paramagnetic fraction, is a titanium and iron-rich mineral, as shown in Figure 4.14. Due to its higher content of iron, it is a more interesting ore than magnetite. This second fraction was separated by inducing a magnetic field of 0.3 to 0.8 amperes, as recommended by the protocol proposed by Londoño (2010) and based on the magnetic susceptibility reported by Rosenblum and Brownfield (1999).

The dark fractions reported in Table 3.1 were also subjected to a heavy material concentration process by panning. The panning process consists of getting rid of the majority of minerals that accompany gold. The gold had already been extracted during the mining stage in our samples, so the gold content was low. However, it is interesting that not all the gold is extracted in the mine due to process failure or inefficiency. This inefficiency is notorious due to the fact that their methods cannot retain gold with laminar or flake shapes because those particles float and are dragged away by the water. An exciting factor during the panning is that small flakes of platinum were found, a mineral of great economic importance that is also not being extracted in the mining process. These platinum flakes were analyzed at the University of Granada in Spain for an age estimation. The result is an approximate age for the platinum flakes of 40 million years [Yakubovich et al., 2023].

So far, 4 minerals have been described, but the most mineralogical variability is found in the diamagnetic fraction. Several techniques were used to analyze this fraction.

Descriptive mineralogy attempts to describe mineral grains according to characteristics that can be observed without using advanced instruments. In this way, the minerals described in Section 4.3.3. were found and identified. The results show that there are abundant quartz grains characterized by their hardness, color, and luster. According to Weiser and Schmidt (1993), Quartz grains are white to yellow, with some alterations due to transport and weathering. Pyrite and Chalcopyrite are recognized by the naked eye by their cubic crystals and grey-to-green metallic colors. They also show polishing by transport, as can be seen in Figures 4.5 and 4.6. These two sulfides are abundant in gold-

bearing deposits because of their similar occurrence and formation [Lucero, 2014]. In the same way, the ferrosilite was recognized by its crystalline structure, where the characteristic arrangement is observed in Figure 4.8.

The minerals described in the previous paragraph were observed in the Stereomicroscope with white light. When UV light was applied to the sample, grains were found to fluoresce with exciting colors, as shown in Figures 4.9c and 4.10b. Based on the fluorescence table proposed by Mineralia (2015), it was determined that the crystals that fluoresce in orange color are zircons and in blue color fluorite. Also, the crystals show alterations due to transport and weathering.

Something interesting we found in the samples is the presence of mercury alloys. These mercury alloys are the product of artisanal mining in the area. The presence of these mercury balls tells us that gold is being recovered by this method, and the tailings have traces of the metal. This discovery is essential to control artisanal mining, which, after this work, is confirmed that it is not a clean operation. The mercury alloys in the samples are distributed in a considerable percentage, so in this work, they have been counted as one more mineral.

In spite of the fact that descriptive mineralogy presents a very good methodology for mineral recognition, we still had doubts about 4 minerals that were recognized by RAMAN spectroscopy. The grains were exposed to a laser, which vibrated their crystalline structure. These vibrations change the molecular state of the mineral, and the waves generated by this vibration are detected [Haskin et al., 1997]. This process allowed us to detect the 4 minerals effectively.

With the help of the CrystalSleuth software developed by NASA for in situ RAMAN analysis of rocks by space exploration equipment, we did correlated on the measured spectra with RRUFF spectra. The RRUFF project collects an extensive database of RAMAN spectra of all materials on the planet. RAMAN analyses have been performed on many minerals and materials, and their exact spectra are available, which can be compared to find the best match in other rocks or materials. In this way, grains were analyzed, and spectra were obtained and compared to the RRUFF spectra to accurately describe minerals such as Brucite, which was mistaken for Chlorite, and Annite, which was mistaken for Biotite. These Berlinite crystals were mistaken for Quartz and Epidote, a heavy mineral that was

mistaken for Beryl.

For further confirmation of the presence of Epidote and Fluorite crystals in the samples, the XPS analysis showed that the compositions of the grains coincide with the theoretical chemical composition of the minerals. Epidote crystal compositions are dominated by Oxygen, Chlorine, Silica, and Aluminium (Fig. 4.27), while Fluorite shows the presence of Magnesium (Fig. 4.28). Up to this point, the entire descriptive mineralogy stage findings are proved and confirmed.

With the help of Doctor Gervilla in Spain, the major, minor, and trace elements analyses on the samples were carried out. We can see that the dominant major elements are Iron, Sulfur, Aluminium, and Magnesium (Table 4.2), which matches the dominance of iron-rich and aluminium-rich minerals found in previous stages. The minor elements, as we can see in Table 4.3, are dominated by Titanium with an 11.1%, and with the presence of a fraction of Platinum, it ends up giving us an exciting result in terms of future exploration. Finally, Table 4.4 shows the much-expected result of trace elements. These results are interesting; they are new and have never been done before in Santiago River samples. We can see the major components are Vanadium, Tin, Cobalt, Zinc, Chromium, Molybdenum, Niobium, Gallium, Thallium, Copper, and Scandium.

Table 4.5 summarizes the elements and their values compared with their abundance in Earth's crust. The Crust Average value is obtained by making an average of various analyses such as Post-Archean Australian Shales (PAAS), North American Shales Composite (NASC), European Shales (ES), and Carbonate-free Loess [Mclennan, 1989, Pourmand et al., 2012]. The elements and values highlighted in yellow are the ones in which the tested value is higher than the average Earth's crust composition. The values in Table 4.5 are represented in parts per million (ppm) where 1 ppm equals 1g/Ton of ore grade; in this work's case, we will talk about Tons of tailing or waste material. McNulty (2022) and Talens (2013) coincide in the fact that the reserves of these minerals in the world are showing ore grades of about 0.02% in normal cases to 10% in the biggest scenarios, such as China. It means that we need at least 2000 g/Ton to consider a site as a potential source [McNulty et al., 2022, Talens Peiró and Villalba Méndez, 2013].

The most abundant element found in this study is Vanadium, with 2438.09 g/Ton, and it is used in the technology and metallurgical industries [ElSevier, 2021]. Followed by

Tin (9.61 g/Ton), which is used in soldering and in the electronics industry [Barry, 2017]. Cobalt (149.08 g/Ton) is essential in the manufacturing of rechargeable lithium-ion batteries in the technology and electronics industry [Crundwell et al., 2011]. Zinc (299.86 g/Ton) is necessary for galvanization and used in manufacturing electronic and pharmaceutical products [Chen et al., 2016]. Chromium (542.56 g/Ton) is a valuable element in metallurgical and stainless steel production [James et al., 1995]. Molybdenum (3.34 g/Ton) is employed in the metallurgical industry and as an additive in high-strength steel alloys [Prasad et al., 1997]. Niobium (43.6 g/Ton) is used in special alloys, particularly in the aerospace and defense industries [Ayanda and Adekola, 2011]. Thallium (2.6 g/Ton) has limited applications due to its toxicity but is still used in trace amounts in the pharmaceutical and electronics industries [Weich et al., 1977]. Scandium (26.73 g/Ton) is crucial in the production of lightweight alloys for aerospace and high-tech applications [Pyrzyńska et al., 2019]. Copper (90.85 g/Ton) is an essential electrical conductor and is widely used in the telecommunications and electronics industries [Pietrzyk and Tora, 2018]. Gallium (20.65 g/Ton) is used in the semiconductor industry and high-tech electronics, making its presence valuable [Lu et al., 2017]. We can see that Vanadium values represent a potential source of this element in the Santiago River sands, and further research is recommended to better understand the reserves and materials.

For the REE reported in Table 4.6, it has been observed that none of them are greater than the Earth's crust concentration. However, the three highest values are Europium (0.31 g/Ton), Thulium (0.1 g/Ton), and Ytterbium (0.63 g/Ton). These results are important for future exploration due to the fact that in this study, we used the mine waste only, and these REEs may be removed in the previous mining stages.

These results suggest that mining waste sands contain various valuable elements essential in various industries, such as technology, pharmaceuticals, and telecommunications. Extracting and processing these elements from mining waste could have significant economic potential and contribute to sustainability by recycling these materials instead of relying on extracting new sources. However, it is also essential to consider the environmental and technical challenges associated with extracting and processing these elements.

Chapter 6

Conclusions

The initial phase of this study involved granulometric separation, a critical step in analyzing the composition of the auriferous sands and gravels along the Santiago River in the Esmeraldas province. This process efficiently divided the samples into smaller fractions, explicitly emphasizing the 120 MESH grain size fraction, which emerged as the most representative. By employing this method, we laid the foundation for subsequent analyses, allowing for a more detailed characterization of the materials.

Following granulometric separation, magnetic separation was conducted to assess the magnetic properties of the materials. The results of this step were particularly revealing, indicating the presence of significant Magnetite content. Magnetite, known to be the primary component of "black sands," is commonly associated with gold-bearing deposits. This discovery suggests that the samples, sourced from artisanal mining tailings, contain a substantial proportion of this heavy fraction. Additionally, Ilmenite, a mineral rich in both titanium and iron, was identified within the paramagnetic fraction. The presence of Ilmenite adds another layer of economic significance to the findings, as it is considered an ore of interest due to its higher iron content than Magnetite.

Panning, a traditional method in mineral exploration, was employed to characterize the samples further. This step confirmed the low gold content in the samples, indicating that the gold had already been extracted during the initial mining stages, but it also yielded an unexpected and exciting discovery. Tiny flakes of platinum were found during panning, marking an essential find with economic implications. An analysis conducted at the University of Granada in Spain estimated the age of these platinum flakes to be

approximately 40 million years, adding an intriguing historical dimension to the study and providing new insights for future research and exploration.

Descriptive mineralogy was crucial in identifying and characterizing various mineral grains in the samples. This technique relied on visual observations and criteria such as hardness, color, luster, and crystal structure. Abundant quartz grains were identified, displaying characteristic white-to-yellow hues with some alterations due to transportation and weathering, as documented in previous studies. Furthermore, pyrite and chalcopyrite were visually recognized by their cubic crystals and metallic gray-to-green colors. These sulfides are frequently encountered in gold-bearing deposits due to their similar formation processes. Ferrosilite, another mineral, was identified based on its distinctive crystalline structure.

Observations were conducted using a stereomicroscope with white light and applying UV light to the samples that revealed fluorescence patterns in various minerals. Notably, crystals fluorescing in orange were identified as zircons, while those fluorescing in blue were determined to be fluorite. These observations added depth to the mineralogical analysis and provided insights into the effects of transport and weathering on the samples.

An unexpected finding in the samples was the presence of mercury alloys. These alloys are indicative of artisanal mining practices in the region. Their presence suggests that gold recovery methods employed by local miners involve mercury, leaving traces of this heavy metal in the tailings. This discovery highlights the importance of monitoring and controlling artisanal mining operations in the area.

To further confirm mineral identities, RAMAN spectroscopy was employed. This technique involved exposing mineral grains to laser light, which caused vibrations in their crystalline structures. The resulting wave patterns were then analyzed. NASA's Crystal-Sleuth software enabled comparisons between measured spectra and established RRUFF spectra, a comprehensive database of RAMAN spectra for various minerals. This analysis clarified the identities of minerals that had previously raised doubts during the descriptive mineralogy phase. Notable identifications included Brucite, Annite, Berlinite, and Epidote.

X-ray Photoelectron Spectroscopy (XPS) was employed to confirm the presence of Epidote and Fluorite crystals in the samples. The chemical compositions of these grains were found to align with the theoretical compositions of the respective minerals. This

confirmation further solidified the findings from the descriptive mineralogy phase.

The major, minor, and trace element analyses conducted with the assistance of Dr. Gervilla in Spain provided valuable insights into the elemental composition of the samples. Major elements such as Iron, Sulfur, Aluminium, and Magnesium dominated the composition, following the prevalence of iron-rich and aluminium-rich minerals previously identified. Minor elements, particularly Titanium, were found in notable concentrations, with a fraction of Platinum added, hinting at promising future exploration opportunities. Trace elements analysis revealed a diverse array of elements, including Vanadium (2438.09 g/Ton), Tin (9.61 g/Ton), Cobalt (149.08 g/Ton), Zinc (299.86 g/Ton), Chromium (542.56 g/Ton), Molybdenum (3.34 g/Ton), Niobium (43.60 g/Ton), Gallium (20.65 g/Ton), Thallium (2.60 g/Ton), Copper (90.85 g/Ton), and Scandium (26.73 g/Ton). We consider Vanadium the most valuable in terms of quantity, and we suggest a potential extraction source in Santiago River areas.

The concentrations of Rare Earth Elements (REE) in the samples did not surpass Earth's crust values, it's worth noting that Europium, Thulium, and Ytterbium exhibited higher concentrations, suggesting potential areas for further exploration.

This comprehensive study of alluvial deposits along the Santiago River has revealed a wealth of valuable insights and potential economic opportunities. Magnetite and Ilmenite, along with the discovery of platinum flakes, underscores the economic significance of these mining waste sands. Moreover, the diverse elemental composition, including Vanadium, Tin, Cobalt, Zinc, Chromium, Molybdenum, Niobium, Gallium, Thallium, Copper, Scandium, and REE, highlights the potential for these materials to serve various industries, ranging from technology and electronics to metallurgy and pharmaceuticals. This study provides a detailed characterization of the materials and emphasizes the importance of responsible and sustainable mining practices, considering both technical and environmental challenges. Further research is recommended to explore the full extent of the reserves and materials, focusing on Vanadium as a valuable resource.

Bibliography

[Andò and Garzanti, 2014] Andò, S. and Garzanti, E. (2014). Raman spectroscopy in heavy-mineral studies. *Geological Society Special Publication*, 386(1):395–412.

[Ayanda and Adekola, 2011] Ayanda, O. S. and Adekola, F. A. (2011). A review of niobium-tantalum separation in hydrometallurgy.

[Barragan et al., 1991] Barragan, J., Ortiz, C., and Merlyn, M. (1991). Placeres auríferos en el Ecuador. *Gisements alluviaux d´or*, pages 23–37.

[Barry, 2017] Barry, B. (2017). Tin processing — Extraction, Refining Uses — Britannica.

[Bevandić et al., 2021] Bevandić, S., Blannin, R., Auwera, J. V., Delmelle, N., Caterina, D., Nguyen, F., and Muchez, P. (2021). Geochemical and mineralogical characterisation of historic zn–pb mine waste, plombières, East Belgium.

[Biswas et al., 2020] Biswas, P. K., Alam, M. S., Hasan, A. M., Ahmed, S. S., and Zaman, M. N. (2020). Geochemical signatures of recent bar deposits in the Tista river, Bangladesh: Implications to provenance, paleoweathering and tectonics. *Journal of Nepal Geological Society*, 60:1–20.

[Briggs, 2005] Briggs, D. (2005). X-ray photoelectron spectroscopy (XPS). *Handbook of Adhesion: Second Edition*, pages 621–622.

[Catlin et al., 1992] Catlin, C. L., Linville, D. W., and Turner, S. (1992). Point counting on the Macintosh. A semiautomated image analysis technique. *Analytical and Quantitative Cytology and Histology*, 14:260–290.

[Chen et al., 2016] Chen, A., Li, M., Qian, Z., Ma, Y., Che, J., and Ma, Y. (2016). Hemimorphite ores: A review of processing technologies for zinc extraction. *JOM*, 68:2688–2697.

[Chen et al., 2022] Chen, W., Yang, Y., Fu, K., Zhang, D., and Wang, Z. (2022). Progress in icp-ms analysis of minerals and heavy metals in traditional medicine. *Frontiers in pharmacology*, 13:891273.

[Crundwell et al., 2011] Crundwell, F. K., Moats, M. S., Ramachandran, V., Robinson, T. G., and Davenport, W. G. (2011). Chapter 30 - production of cobalt from the copper–cobalt ores of the central african copperbelt. In Crundwell, F. K., Moats, M. S., Ramachandran, V., Robinson, T. G., and Davenport, W. G., editors, *Extractive Metallurgy of Nickel, Cobalt and Platinum Group Metals*, pages 377–391. Elsevier, Oxford.

[Dietzek et al., 2018] Dietzek, B., Cialla, D., Schmitt, M., and Popp, J. (2018). Introduction to the fundamentals of raman spectroscopy. *Springer Series in Surface Sciences*, 66:47–68.

[ElSevier, 2021] ElSevier (2021). Chapter 3 - vanadium mineral resources. In Yang, B., He, J., Zhang, G., and Guo, J., editors, *Vanadium*, pages 33–58. Elsevier.

[Frezzotti et al., 2012] Frezzotti, M. L., Tecce, F., and Casagli, A. (2012). Raman spectroscopy for fluid inclusion analysis. *Journal of Geochemical Exploration*, 112:1–20.

[Garzanti et al., 2011] Garzanti, E., Andó, S., France-Lanord, C., Censi, P., Vignola, P., Galy, V., and Lupker, M. (2011). Mineralogical and chemical variability of fluvial sediments 2. Suspended-load silt (Ganga-Brahmaputra, Bangladesh). *Earth and Planetary Science Letters*, 302(1-2):107–120.

[Griffith, 1969] Griffith, W. P. (1969). Raman Spectroscopy of Minerals. *Nature 1969 224:5216*, 224:177–178.

[Haskin et al., 1997] Haskin, L. A., Wang, A., Rockow, K. M., Jolliff, B. L., Korotev, R. L., and Viskupic, K. M. (1997). Raman spectroscopy for mineral identification and quantification for in situ planetary surface analysis: A point count method. *Journal of Geophysical Research: Planets*, 102(E8):19293–19306.

[James et al., 1995] James, B. R., Petura, J. C., Vitale, R. J., and Mussoline, G. R. (1995). Hexavalent chromium extraction from soils: a comparison of five methods. *Environmental Science & Technology*, 29(9):2377–2381.

[Jamieson et al., 2015] Jamieson, H. E., Walker, S. R., and Parsons, M. B. (2015). Mineralogical characterization of mine waste. *Applied Geochemistry*, 57:85–105.

[Jelenová et al., 2018] Jelenová, H., Majzlan, J., Amoako, F. Y., and Drahota, P. (2018). Geochemical and mineralogical characterization of the arsenic-, iron-, and sulfur-rich mining waste dumps near Kaňk, Czech Republic. *Applied Geochemistry*, 97:247–255.

[Klein et al., 2002] Klein, C., Hurlbut, C. S., and Dana, J. D. (2002). Manual of Mineral Science (22nd Ed.) (Manual of Mineralogy).pdf.

[Kloprogge and Wood, 2020] Kloprogge, J. T. and Wood, B. J. (2020). *Handbook of Mineral Spectroscopy: Volume 1: X-ray Photoelectron Spectra.*

[Larrea et al., 2014] Larrea, M. L., Martig, S. R., Castro, S. M., Aliani, P. A., and Bjerg, E. A. (2014). Rock.AR - A Point Counting application for Petrographic Thin Sections.

[Londoño et al., 2010] Londoño, J., Mojica, J., Molano, J., Cañón, R., Mosquera, S., and Ruiz, S. (2010). *Ténicas mineralógicas, químicas y metalúrgicas.*

[López-Males et al., 2020] López-Males, G. G., Aiglsperger, T., Pujol-Solà, N., and Proenza, J. A. (2020). New mineralogical data on platinum-group minerals from the Río Santiago alluvial placer, Esmeraldas province, Ecuador. *Boletin de la Sociedad Geologica Mexicana*, 72(3).

[Lu et al., 2017] Lu, F., Xiao, T., Lin, J., Ning, Z., Long, Q., Xiao, L., Huang, F., Wang, W., Xiao, Q., Lan, X., et al. (2017). Resources and extraction of gallium: A review. *Hydrometallurgy*, 174:105–115.

[Lucero, 2014] Lucero, G. (2014). Optimización De Los Procesos De Extracción De Grava Aurífera Y Proceso De Lavado Del Frente "El Porvenir" En El Proyecto Río Santiago, Empresa Nacional Minera.

[Mclennan, 1989] Mclennan, S. M. (1989). Chapter 7 S. M. McLennan Rare Earth Elements in Sedimentary Rocks: Influence of Provenance and Sedimentary Processes. *Reviews in Mineralogy Geochemistry*.

[McNulty et al., 2022] McNulty, T., Hazen, N., and Park, S. (2022). Processing the ores of rare-earth elements. *MRS Bulletin*, 47(3):258–266.

[Mikhlin, 2020] Mikhlin, Y. (2020). X-ray photoelectron spectroscopy in mineral processing studies. *Applied Sciences (Switzerland)*, 10(15):17–24.

[Mineralia.org, 2015] Mineralia.org (2015). Minerales fluorescentes.

[Ministerio del Ambiente, 2020] Ministerio del Ambiente (2020). Línea de base nacional para la Minería Artesanal y en Pequeña Escala de Oro en Ecuador, Conforme la Convención de Minamata sobre Mercurio. *Organización de las Naciones Unidas para el Desarrollo Industrial*, pages 1–89.

[Moor et al., 2001] Moor, C., Lymberopoulou, T., and Dietrich, V. J. (2001). Determination of heavy metals in soils, sediments and geological materials by icp-aes and icp-ms. *Microchimica Acta*, 136:123–128.

[Nasdala et al., 2004] Nasdala, L., Smith, D. C., Kaindl, R., Ziemann, M. A., Beran, A., Libowitzky, E., et al. (2004). Raman spectroscopy: analytical perspectives in mineralogical research. *Spectroscopic methods in mineralogy*, 6:281–343.

[Olesik, 2000] Olesik, J. W. (2000). 1991-Icp Oes Et Icp Ms. *Analytical Chemistry*, 63(1):12–21.

[Pietrzyk and Tora, 2018] Pietrzyk, S. and Tora, B. (2018). Trends in global copper mining–a review. In *IOP conference series: materials science and engineering*, volume 427, page 012002. IOP Publishing.

[Pillajo Gavidia, 2008] Pillajo Gavidia, E. (2008). Evaluación del potencial aurífero aluvial en ecuador. pages 1–12.

[Pourmand et al., 2012] Pourmand, A., Dauphas, N., and Ireland, T. J. (2012). A novel extraction chromatography and MC-ICP-MS technique for rapid analysis of REE, Sc

and Y: Revising CI-chondrite and Post-Archean Australian Shale (PAAS) abundances. *Chemical Geology*, 291:38–54.

[Prasad et al., 1997] Prasad, P., Mankhand, T., and Prasad, A. (1997). Molybdenum extraction process: an overview. *NML technical journal*, 39(2):39–58.

[Pyrzyńska et al., 2019] Pyrzyńska, K., Kilian, K., and Pegier, M. (2019). Separation and purification of scandium: From industry to medicine. *Separation & Purification Reviews*, 48(1):65–77.

[Raman and Krishnan, 1928] Raman, C. V. and Krishnan, K. S. (1928). A new type of secondary radiation [11].

[Rigaku Corporation, 2023] Rigaku Corporation (2023). MiniFlex — Rigaku Global Website.

[Rosenblum and Brownfield, 1999] Rosenblum, S. and Brownfield, I. K. (1999). Magnetic Susceptibilities of Minerals - Report for U.S. Geological Survey. *U.S. Department of The Interior U.S. Geological Survey*, 1(703):1–33.

[RRUFF Project, 2016] RRUFF Project (2016). Database of Raman spectroscopy, X-ray diffraction and chemistry of minerals.

[Seyama et al., 2013] Seyama, H., Soma, M., and Theng, B. K. (2013). *X-Ray Photoelectron Spectroscopy*, volume 5. Elsevier Inc., 1 edition.

[Talens Peiró and Villalba Méndez, 2013] Talens Peiró, L. and Villalba Méndez, G. (2013). Material and energy requirement for rare earth production. *Jom*, 65(10):1327–1340.

[Tamay, 2018] Tamay, J. V. (2018). *Estructura de cuencas intramontañosas del sur de Ecuador en relación con la tectónica de la Cordillera de los Andes a partir de datos geofísicos y geológicos.*

[Techera and Arrighetti, 2002] Techera, J. and Arrighetti, R. (2002). Informe Geologigo / Yacimentologico Del Deposito De Arenas Negras (Minerales Pesados) De Aguas Dulces. pages 10–11.

[Tyler and Yvon, 2003] Tyler, G. and Yvon, J. (2003). ICP-OES , ICP-MS and AAS Techniques Compared. *Technical note 05: ICP Optical Spectroscopy*, (3):1–11.

[Weich et al., 1977] Weich, H. F., Strauss, H. W., and Pitt, B. (1977). The extraction of thallium-201 by the myocardium. *Circulation*, 56(2):188–191.

[Weiser and Schmidt-Thome, 1993] Weiser, T. and Schmidt-Thome, M. (1993). Platinum-group minerals from the Santiago River, Esmeraldas Province, Ecuador. *Canadian Mineralogist*, 31(1):61–73.

[Welsh, 2021] Welsh, D. A. (2021). Instructions For Point Counts. *Atlas Des Oiseaux Nicheurs Ontario Breeding Bird Atlas*, (June):1–6.

[Yakubovich et al., 2023] Yakubovich, O. V., Stuart, F. M., Ivanova, E. S., and Gervilla, F. (2023). Constant 4He Concentration and 190Pt-4He age of Detrital Pt-Alloy Grains from the Santiago River, Ecuador: Potential as a 4He Mineral Reference Material. *Geostandards and Geoanalytical Research*, (3):0–1.